AFFDL-TR-70-31

HYPERSONIC SURFACE PRESSURE AND HEAT TRANSFER ON SLENDER BODIES IN VARIABLE COMPOSITION AND NONEQUILIBRIUM ATMOSPHERES

D. J. HARNEY

S. L. PETRIE

FOREWORD

This final technical report was prepared by D. J. Harney and S. L. Petrie of the Aeronautical and Astronautical Research Laboratory, Department of Aeronautical and Astronautical Engineering for the Research Foundation of The Ohio State University under Contract AF33(615)-69-C-1077, "Similitude Studies for Slender Bodies in Nonequilibrium Flows."

The contract was initiated under Project No. 1426, "Experimental Simulation for Flight Mechanics," Task No. 142604, "Theory of Dynamic Simulation of Flight Environment." The work was administered by the Air Force Flight Dynamics Laboratory, Wright-Patterson Air Force Base, Ohio, Mr. Edmund Brown-Edwards (FDME), Project Engineer.

The work was accomplished during the period 1 September 1968 through 31 September 1969.

The report was submitted by the authors in October 1969.

This technical report has been reviewed and is approved.

PHILLIP P. ANTONATOS
Chief, Flight Mechanics Division
Air Force Flight Dynamics Laboratory

ABSTRACT

The aerodynamic testing of slender bodies in high energy wind tunnels is complicated by the effects of the nonequilibrium expansion process in the wind tunnel nozzle. The atmosphere that a model sees varies in composition dependent upon the degree of nonequilibrium. This variation affects the inviscid flow field through changes in the ratio of specific heats and the viscous equations by changes in the transport as well as the thermodynamic properties of the gas. Within the limitations of hypersonic small disturbance theory the inviscid and viscous equations are formulated with a minimal dependence on Mach number and in a way that brings out their explicit dependence on the thermodynamic and transport properties of the gas. The resulting gas property parameters then are calculated for air-argon mixtures, air-helium mixtures, and frozen dissociate air. These parameters appear to provide a realistic estimate of the effect of a variable atmosphere on surface pressure and heat transfer based on the current series of tests on sharp cones and flat plates in air-argon mixtures and in a low pressure arc tunnel. In addition, the present experiments and comparative experiments in other facilities demonstrate a result of more general interest, namely, that the Mach number is not a dominant parameter in slender body viscous hypersonic aerodynamics.

TABLE OF CONTENTS

LIST OF FIGURES

LIST OF SYMBOLS

b_i	mole numbers
C	Chapman-Rubesin constant, $C = \frac{\bar{\mu}}{\mu_\infty}\frac{T_\infty}{\bar{T}_\infty}$
C_f	skin friction coefficient $\frac{\tau_w}{q_\infty}$
C_H	heat transfer rate coefficient $\frac{\dot{q}}{\rho_\infty u_\infty (H_o - H_w)}$
C_p	pressure coefficient $\frac{p - p_\infty}{q_\infty}$
$\mathcal{C}$	specific heat of model material
$\mathcal{C}_p$	gas specific heat at constant pressure
$\mathcal{C}_{p_o}$	specific heat at standard T and p, $\mathcal{C}_{p_o} = 6000 \frac{ft^2}{sec^2\text{-}^\circ R}$
F	variable gas composition parameter (See Eq. 14)
G	variable gas composition parameter (See Eq. 15)
H_o	total gas enthalpy
H_w	gas enthalpy at the surface
k	thermal conductivity
M	freestream Mach number
$\mathcal{M}$	molecular weight
n	power law exponent, $p \propto x^{-n}$

LIST OF SYMBOLS (continued)

p	pressure, lb_f/ft^2
p_{t_2}	wind tunnel pitot pressure
q	dynamic pressure
$\dot{q}$	heat transfer rate
r	radius of axisymmetric model
R	specific gas constant for undissociated air = 1716 $\frac{ft^2}{sec^2\text{-}^\circ R}$
$\mathcal{R}$	universal gas constant
S_o	wind tunnel reservoir entropy
St	Stanton number, $\dot{q}/\rho_\infty u_\infty C_p(T_{aw}-T_w)$
t	time to melt phase-change coating, seconds
T	gas temperature, degrees Rankine
$\overline{T}$	reference temperature (See Eq. 10)
T_{aw}	adiabatic wall temperature
T_i	initial surface temperature of model
T_p	melting temperature of phase-change coating
u	gas velocity, ft/sec

LIST OF SYMBOLS (continued)

x	streamwise distance, feet
x^*	stretched streamwise coordinate (See Eq. 7 and 9)
$\bar{x}$	stretched streamwise coordinate (See Eq. 22)
α	angle-of-attack on windward surface
β	mole fraction of atomic additive
γ	ratio of specific heats
γ_o	ratio of specific heats for air at standard T and p
θ	local flow inclination angle, radians
δ^*	boundary layer displacement thickness
θ_w	local inclination of surface to freestream, radians
Θ	$(T_p - T_i)/(T_{aw} - T_w)$
μ	gas viscosity, lb_f-sec/ft^2
$\bar{\mu}$	gas viscosity at the reference temperature
τ	radial heat conduction parameter = $\alpha t/r^2$
τ_w	surface shear stress lb_f/ft^2
ρ	gas density, slugs/ft^3

LIST OF SYMBOLS (continued)

$\bar{\chi}$	viscous interaction parameter
c	properties related to a cone
e	conditions external to the boundary layer
i,j	summation subscripts for gas species
o	reservoir properties (except for the reference gas properties ℓ_o and ℓ_{p_o})
w	wall conditions
∞	freestream conditions

I. INTRODUCTION

The aerodynamic characteristics of slender bodies remain of interest because of the superior performance of such vehicles for certain types of hypervelocity missions. Adequate estimation of their performance requires knowledge of the appropriate similarity parameters so that free flight and wind tunnel data can be correlated.

The degree of complexity of the similitude considerations depends upon the detailed body shape and the type of ground-based test facility employed. For example, at Mach numbers greater than 4, blunt bodies display Mach and Reynolds number independence and the detailed thermochemical state of the test gas has little influence on the surface pressure distribution.[1,2] Hence, reliable simulation of blunt-body flows can be obtained over the majority of the operating range of high enthalpy wind tunnels with little regard for the detailed nature of the freestream flow.

While viscous effects and freestream nonequilibrium have negligible effects in blunt-body flows, their influences on slender body aerodynamics may be sizeable. This is due, in part, to the weaker shock-wave system on a slender body and the attendant absence of any region for equilibration of the chemical and thermodynamic state of the gas prior to its expansion about the body. Further, viscous interaction effects play a much more important role in slender body flows. Should nonequilibrium be present in the flow upstream of a slender body, the alterations of the transport properties may influence the viscous interaction phenomena and, hence, change the pressure distribution. For blunt bodies, transport processes have second-order effects on the pressure distribution. However, in slender body flows, the effects of changing transport properties need to be examined in addition to any direct influences of chemical and thermodynamic nonequilibrium to properly interpret pressure and heat transfer data.

The similitude of hypersonic flow may be analyzed in a number of ways, the most popular being the study of the governing differential equations. Beginning with the basic hypersonic similarity of Tsien this approach has been applied effectively with an increasing degree of complexity for the inviscid flow field in Refs. 3 through 8 and extended to include the interacting effects of a thick boundary layer in Refs. 9 through 12. From this type of similitude analysis the parameters of interest, such as the surface pressure coefficient, are established in terms of some unspecified functional dependence on a minimum number of nondimensional parameters.

Another effective approach to hypersonic similitude and the one employed in this study is the generalization of simple solutions. Tangent-wedge and tangent-cone theory allows the solutions for the flows over a wedge and cone to be extended quite accurately to flows over planar and axisymmetric bodies. This approach at least establishes the

significant similarity parameters and permits their formulation in a variety of ways. In certain cases, accurate predictions of the aerodynamic unknowns can also be obtained.

The similitude for high enthalpy test facilities is complicated by the existence of thermodynamic and chemical nonequilibrium in the nozzle expansion process. It is found that the gas in the test section has a chemical composition and thermodynamic energy distribution in internal energy modes which vary with the test condition. Hence, the detailed state of the gas within the body flow field is coupled strongly to the degree of nonequilibrium in the freestream.

Over a large range of operating conditions of high enthalpy wind tunnels, chemical and vibrational energy freezing will occur in the nozzle flow at low supersonic Mach numbers. The test body thus will be immersed in a free-stream flow comprised of a mixture of atoms and molecules which behaves as a perfect gas with a constant ratio of specific heats (γ) greater than the atmospheric value of 1.4. If the body is sufficiently slender, the low density levels associated with the weak shock-wave system and the small flow transit time accompanying the high flow velocity result in an insufficient number of intermolecular collisions for chemical and thermodynamic reactions to occur within the body flows are expected to be manifested as a simple γ effect which may be coupled with viscous interaction phenomena.[2] The viscous effects are governed by the transport properties which may be altered by nonequilibrium in the nozzle expansion.

The general similarity considerations for nonequilibrium flow have been analyzed by Inger.[8] When viscous effects are coupled with the influences of nonequilibrium in the chemical and thermodynamic energy states, a general treatment of similarity appears to be hopeless. However, because of the character of slender body flows, it can be assumed that the chemical state and thermodynamic energy level in internal degrees of freedom remain fixed throughout much of the aerodynamic flow field of interest.

As shown in Ref. 13 the usual hypersonic small disturbance theory can be applied to slender bodies in high enthalpy flows when the assumption of frozen chemistry is applicable. Correlations based on similarity parameters developed from this theory compare favorably with test data from perfect gas facilities. However, few data are available from high enthalpy facilities. The purpose of the studies reported here is to examine the similarity rules which govern the aerodynamic performance of slender bodies in nonequilibrium flows with variable freestream transport properties. The applicability of the correlating parameters is examined with pressure and heat transfer data obtained with sharp cones and sharp flat plates in the OSU variable atmosphere and arc-heated wind tunnels.

The theoretical analyses are summarized in Section II. The

experimental data and methods of analysis are presented in Section III. Correlations of the data are discussed in Section IV.

II. THEORETICAL ANALYSES

The analysis is limited to hypersonic flows where continuum theory and no-slip boundary conditions are applicable. Although the experiments show a departure from strong viscous interaction which may be interpreted as the onset of merging of the viscous layer with a diffused shock layer, molecular effects and the "leading-edge problem" are not included in this study. Within these limitations the objectives are to evaluate the effects of variable gas properties of tailored perfect-gas atmospheres on the aerodynamic performance of slender bodies and to extend these results to the case of a nonequilibrium freestream.

As in Ref. 13, the explicit appearance of the Mach number in the similarity parameters is avoided. In perfect gases, the Mach number is determined solely by the local nozzle area ratio and the ratio of specific heats. However, in high enthalpy test facilities, the speed of sound in the test gas may vary greatly with the changing gas composition. Hence, the Mach number is an ill-defined quantity in many nonequilibrium flow fields.

A. INVISCID FLOW FIELD

For the inviscid flow field we restrict the analysis to bodies with sharp leading edges or with very small degrees of bluntness where blunting effects are upstream of the region under consideration. With the Mach number assumed large, tangent-wedge and tangent-cone theories can be applied. Hence, we neglect longitudinal curvature effects and the entropy layer and concentrate on an accurate description of the surface pressure for the flow over wedges and cones.

The usual assumptions of hypersonic small disturbance theory are made:

$$\left.\begin{aligned} M &\gg 1 \\ \sin\theta &\ll 1 \\ M\sin\theta &\geq 1 \end{aligned}\right\} \qquad (1)$$

Within these constraints the equations for the surface pressure on a wedge and a cone are

Wedge

$$\frac{p}{q_\infty} = 1.015(1 + \gamma) \sin^2 \theta + \frac{2.286\ \gamma + 1}{\gamma + 1} \frac{p_\infty}{q_\infty} \qquad (2)$$

Cone

$$\frac{p_c}{q_\infty} = 1.800(1 + 0.12\ \gamma) \sin^2 \theta + \frac{1.370\ \gamma + 1}{\gamma + 1} \frac{p_\infty}{q_\infty} \qquad (3)$$

The expression for the surface pressure on a wedge is obtained by linearizing the small disturbance equation of Linnell[14] and then evaluating the numerical coefficients by matching the exact oblique shock values with a minimum error over the range $1 \leq M \sin \theta < \infty$. With the functional form of Eq. (2) as a guide the surface pressure on a cone was determined from a sequence of computer solutions to the Taylor-Maccoll equation which sought out the numberical coefficients to minimize deviations from the exact solution over the range $1 \leq M \sin \theta < \infty$. Over this range the result is accurate to well within 1% with an allowable range of the individual variables of $M \geq 5$, $\sin \theta \leq \frac{1}{2}$ and $1.20 \leq \gamma \leq 1.67$.

In Eqs. (2) and (3) the effect of a variable composition atmosphere, contained in the frozen ratio of specific heats, γ, is given explicitly and the angle θ is taken as the sum of the angle of inclination of the wall to the freestream, θ_w, and the displacement angle of the boundary layer, $d\delta^*/dx$.

Throughout this analysis the only direct dependence of the equations on Mach number is contained in the second term on the right hand sides of Eqs. (2) and (3). In practice, Mach number and the associated value of p_∞/q_∞ are inferred from measured wind tunnel reservoir conditions, the test section pitot pressure, and a theoretical model for the nozzle expansion process. For high temperature wind tunnels the expansion usually is a nonequilibrium process and the test section properties cannot be obtained accurately. If p_∞ could be measured with some degree of confidence, for example, through spectroscopic measurements of temperature and density, the Mach number would not have to be considered explicitly if it is sufficiently high to satisfy the limitations of hypersonic small disturbance theory. Further; with an independent measure of the freestream pressure it is possible to formulate modified pressure coefficients from Eqs. (2) and (3) which are independent of Mach number in the form $[p - f(\gamma)p_\infty]/q_\infty$. Note that in the usual theory $f(\gamma) = 1$, while here $f(\gamma)$ is given by $(2.286\ \gamma + 1)/(\gamma + 1)$ for a wedge and $(1.370\ \gamma + 1)/(\gamma + 1)$ for a cone.

B. VISCOUS FLOW FIELD

The equations used for skin friction and for the displacement effect of the boundary layer are essentially the same as those derived in Ref. 13. The momentum integral equation for small pressure gradients uses

the Blasius result for planar flow in the form

$$\frac{d\theta}{dx} = \frac{1}{2} C_{f_e} = \frac{1}{2} \frac{(0.664)^2}{Re_\theta} \tag{4}$$

and for cone flow as

$$\frac{d\theta}{dx} + \frac{\theta}{x} = \frac{1}{2} C_{f_e} = \frac{1}{2} \frac{(0.664)^2}{Re_\theta} \tag{5}$$

Integration of the momentum equations, a transformation to a compressible boundary layer employing reference properties, and a hypersonic limit approximation for δ^*/θ gives (Ref. 13) for planar flow where the stretched

$$\frac{d\delta^*}{dx} = 1.730 \left(\overline{Re}_{x^*}\right)^{-1/2} \tag{6}$$

axial coordinate which accounts for the upstream pressure history and produces local flat plate similarity is

$$x^* = p \int_o^x \frac{1}{p} \, dx \tag{7}$$

For axisymmetric flow (Ref. 13) we obtain

$$\frac{d\delta^*}{dx} = 1.730 \left(\overline{Re}_{x_c^*}\right)^{-1/2} \left[1 - 2 \frac{x_c^*}{x}\right] \tag{8}$$

and

$$x_c^* = \frac{p}{x^2} \int_o^x \frac{x^2}{p} \, dx \tag{9}$$

The Reynolds number $\overline{Re}_{x^*}$ is formed from reference gas properties within the boundary layer based on the reference temperature

$$\overline{T} = 0.095 \frac{u_e^2}{c_p} + 0.5 \, (T_e + T_w) \tag{10}$$

and the viscosity is assumed to vary according to the Sutherland relation in the form

$$\mu = 2.27 \times 10^{-8} \sqrt{T}\left[\frac{1}{1 + 200/T}\right] \tag{11}$$

where T is in degrees Rankine. Employing the small disturbance assumption that $u_e \approx u_\infty$, the results for planar flow give the growth of the displacement thickness, the skin friction coefficient, C_f, and assuming Reynolds analogy for unit Prandtl number, the heat transfer coefficient as

$$\frac{d\delta^*}{dx}\sqrt{p/q_\infty} = 3.84 \times 10^{-6} F\left[1 + 2.6\,\frac{T_w}{T_o}\right]^{3/4} (\rho_\infty x^*)^{-1/2} \tag{12}$$

and

$$\frac{C_H}{\sqrt{p/q_\infty}} \approx \frac{C_f/2}{\sqrt{p/q_\infty}} = 1.32 \times 10^{-5}\, G(\rho_\infty x)^{-1/2} \tag{13}$$

All of the variations in the thermodynamic and transport properties of the gas are contained in the factors F and G which are defined as

$$F = F'/F'_{air} \qquad \text{where} \qquad F' = \frac{(R\mu)^{1/2}}{\rho_p^{3/4}} \tag{14}$$

$$G = G'/G'_{air} \qquad \text{where} \qquad G' = \left(\frac{\mu}{R}\right)^{1/2} (\rho_p)^{1/4} \tag{15}$$

In Eq. (12) the numercial values in the expression $\left[1 + 2.6\,\frac{T_w}{T_o}\right]$ are derived principally from the form assumed for the reference temperature, Eq. (10). While the reservoir temperature, T_o, applies strictly to the perfect gas wind tunnel case, the cases of free flight and the high energy wind tunnel may be approximated by using H_w/H_o in place of T_w/T_o. For the axisymmetric case, Eqs. (12) and (13) become

$$\frac{d\delta_c^*}{dx}\sqrt{p/q_\infty} = 3.84 \times 10^{-6} F\left[1 + 2.6\,\frac{T_w}{T_o}\right]^{3/4} (\rho_\infty x_c^*)^{-1/2}\left[1 - 2\,\frac{x_c^*}{x}\right] \tag{16}$$

$$\frac{C_H}{\sqrt{p/q_\infty}} \approx \frac{C_f/2}{\sqrt{p/q_\infty}} = 1.32 \times 10^{-5}\sqrt{3}\, G(\rho_\infty x)^{-1/2} \tag{17}$$

For simplicity, the transformed axial coordinate is used only in the displacement thickness growth equation, which combines with the inviscid equation in the calculation of the surface pressure. In addition, the comparatively small effect of wall temperature on skin friction and heat transfer has been neglected in Eqs. (13) and (17). For skin friction and heat transfer, these two neglected effects are of the same order of magnitude and compensating. Higher values of T_w/T_o reduce the heat transfer and skin friction coefficients and simultaneously drive the induced pressure toward strong interaction which, in turn, has the effect of increasing the skin friction.

A useful and often reasonable approximation to the pressure variation on a slender body is the assumption of a power law variation of the form $p \propto x^{-n}$. In the strong viscous interaction regime on a flat plate, for example, $n = \frac{1}{2}$. When the power law approximation is permissible, the displacement thickness growth equations may be written with the actual physical coordinate, x, for planar flow as

$$\frac{d\delta^*}{dx}\sqrt{p/q_\infty} = \sqrt{n+1}\,(3.84 \times 10^{-6})F\left[1 + 2.6\,\frac{T_w}{T_o}\right]^{3/4}(\rho_\infty x)^{-1/2} \qquad (18)$$

and for axisymmetric flow as

$$\frac{d\delta_c^*}{dx}\sqrt{p/q_\infty} = \frac{n+1}{\sqrt{n+3}}\,(3.84 \times 10^{-6})F\left[1 + 2.6\,\frac{T_w}{T_o}\right]^{3/4}(\rho_\infty x)^{-1/2} \qquad (19)$$

C. EXPLICIT SOLUTIONS

With further approximations, the inviscid and viscous equations may be combined to give explicit expressions for the pressure coefficient on a planar or axisymmetric body. In general, this results in a quadratic equation for the quantity $\sqrt{p/q_\infty}$ with a solution which yields little simplification and a loss in accuracy. However, for a flat plate at zero angle of attack, the solution for the pressure coefficient (Ref. 13) reduces quite accurately to

$$C_p = 3.87 \times 10^{-6}(\gamma + 1)^{1/2}F\left[1 + 2.6\,\frac{T_w}{T_o}\right]^{3/4}(\rho_\infty x^*)^{-1/2} \qquad (20)$$

A useful linearized approximation for x^* for departures from the strong interaction limit was found to be (Ref. 13)

$$\frac{x^*}{x} = \frac{2}{3}\left[1 + \frac{1}{4}\,\frac{p_\infty}{p - p_\infty}\right] \qquad (21)$$

For weak interactions, $x^* = x$.

D. DISCUSSION OF SIMILARITY PARAMETERS

The viscous equations derived above are equivalent to the results obtained from a similarity analysis of the boundary layer equations under the appropriate coordinate transformations. Two major differences require discussion. These differences appear in the form of the stretching transformation of the axial coordinate and in the dimensional character of the simplified rarefaction parameter ($\rho_\infty x$).

In this analysis we derive the growth rate of the boundary layer displacement thickness on a flat plate, $d\delta^*/dx$, as the basic quantity of interest in terms of the stretched axial coordinate.

$$x^* = p \int_0^x \frac{1}{p}\, dx \tag{7}$$

This contrasts with the stretching transformation developed in Refs. 11 and 12 where, using a similarity transformation of the boundary layer coordinates, the displacement thickness, δ^*, is written as a function of another stretched axial coordinate. Within the assumption employed here this latter coordinate can be defined as

$$\bar{x} = \frac{1}{p} \int_0^x p\, dx \tag{22}$$

For this case we have $\delta^* \sim (\bar{x})^{-1/2}$ as compared to the present analysis that gives $d\delta^*/dx \sim (x^*)^{-1/2}$. The two results are essentially equivalent; this is most easily demonstrated by assuming a general power law for the pressure variation. That is, if we let $p \sim x^{-n}$, both cases give $d\delta^*/dx \sim x^{(n-1)/2}$. Thus, the correction for variations in the upstream pressure (i.e., the axial stretching transformation) assumes a slightly different form depending on whether local flat plate similarity is desired in the displacement thickness, δ^*, or in its growth rate, $d\delta^*/dx$. Here, the latter is of principal interest and we employ Eq. (7).

The second principal difference of note is the use of a simple dimensional rarefaction parameter. Although the complete equations are nondimensional, the parameter $(\rho_\infty x^*)^{-1/2}$ is dimensional. If desired, it can be nondimensionalized in a variety of ways. This may result in a simplification or may produce unnecessary complications depending on the application of the results. Certainly in applying the results to the calculation of flight performance the density altitude is a fundamental variable. Since ρ_∞ appears explicitly, there is no need in this case to nondimensionalize the result in terms of free stream Mach number and Reynolds number. On the other hand for theoretical analyses using the governing differential equations it is clearly of advantage to employ nondimensional parameters and variables throughout.

Using the Sutherland viscosity relation for viscosity, Eq. (11), we may transform the viscous equations to a form employing nondimensional parameters by the ralation

$$(\rho_\infty x)^{-1/2} = \sqrt{\frac{M}{Re_{x,\infty}}} \frac{(\gamma R)^{1/4}}{(2.27 \times 10^{-8})^{1/2}} \left[1 + \frac{200}{T_\infty}\right] \tag{23}$$

or, alternately, the equation may be rephrased in terms of the Knudsen number where the mean free path is

$$\lambda_\infty = \frac{16}{5} \frac{\mu_\infty}{\rho_\infty (2\pi R T_\infty)^{1/2}} \tag{24}$$

giving

$$Kn = \frac{\lambda_\infty}{x} = \frac{16}{5} \sqrt{\frac{\gamma}{2\pi}} \frac{M}{Re_{x,\infty}} \tag{25}$$

Thus, the rarefaction parameter can be reduced to either $\sqrt{M/Re}$ or $\sqrt{Kn}$ with a multiplying factor dependent on gas properties.

If a nondimensional form of the hypersonic viscous interaction parameter is needed, the following form for planar flow expressed in terms of the freestream Knudsen number is suggested

$$\frac{d\delta^*}{dx} \sqrt{p/q_\infty} = 0.370 \left(\frac{\gamma - 1}{\gamma}\right)^{3/4} \left[1 + 2.6 \frac{T_w}{T_o}\right]^{3/4} \left[1 + \frac{200}{T_\infty}\right]^{1/2} \sqrt{Kn} \tag{26}$$

where $Kn = \lambda_\infty / x^*$. With all of the parameters nondimensionalized, the effect of a variable composition or nonequilibrium freestream appears to reduce to a simple γ effect. However, the variation in the thermodynamic and transport properties must be considered in the calculation of the Knudsen number.

As a consequence of requiring that the basic rarefaction parameter be nondimensionalized in terms of freestream variables, we have introduced into Eqs. (23) and (26) the temperature dependence of the freestream collision cross section $(1 + 200/T_\infty)$. This factor can be suppressed by employing the Chapman-Rubesin constant which is evaluated here at the reference temperature (Eq. 10). That is, we define

$$C = \frac{\bar{\mu}}{\mu_\infty} \frac{T_\infty}{\bar{T}} \tag{27}$$

and assume that the actual viscosity variation follows the Sutherland relation, Eq. (11). Our dimensional rarefaction parameter can now be written as

$$(\rho_\infty x)^{-1/2} = 3.69 \times 10^3 \frac{(\gamma R)^{1/2}}{C_p^{1/4}} \left[1 + 2.6 \frac{T_w}{T_o}\right]^{1/4} \frac{M\sqrt{C}}{\sqrt{Re_{x^*,\infty}}} \tag{28}$$

and the growth of the planar boundary layer is described by

$$\frac{d\delta^*}{dx} \sqrt{p/q_\infty} = 0.233 \frac{\gamma - 1}{\sqrt{\gamma}} \left[1 + 2.6 \frac{T_w}{T_o}\right] \frac{M\sqrt{C}}{\sqrt{Re_{x^*,\infty}}} \tag{29}$$

Equation (29) offers some simplification in format. However, it should be recognized in comparing Eq. (29) with Eq. (26) that although the temperature dependence of the free stream collision cross section does not appear explicitly in Eq. (29) its variation must still be considered in calculating the "constant" C. In addition, since C as defined by Eq. (27) is inversely proportional to Mach number, Eq. (29) contains an extraneous Mach number dependence.

At least for the purpose of the present studies the attempt to nondimensionalize the basic rarefaction parameter $(\rho_\infty x)^{-1/2}$ leads only to additional complications. For this reason we retain the practical simplicity of this dimensional parameter while recognizing that a nondimensional parameter might be preferred in certain other types of analysis.

E. VARIABLE COMPOSITION AND NONEQUILIBRIUM ATMOSPHERES

For the inviscid flow field about a slender body, the thermodynamic properties of the gas enter only through the frozen ratio of specific heats, γ. In the viscous equations, because we use a simple reference temperature transformation of the Blasius solution, all of the pertinent gas properties appear explicitly and are contained solely in the parameters F and G. The various influences of variable composition and nonequilibrium atmospheres are discussed below.

1. Thermodynamic Properties

The gas is assumed to be a mixture of diatomic molecules and some mole fraction, β, of an atomic species due either to the ineffectiveness of recombination in a nonequilibrium expansion or to purposeful

addition to form a tailored atmosphere. Because it is assumed that the flow is frozen in chemistry and vibration, the ratio of specific heats is taken as

$$\gamma = \frac{3.5 - \beta}{2.5 - \beta} \tag{30}$$

and

$$c_p = R[3.5 - \beta] \tag{31}$$

where R is the specific gas constant for the mixture.

$$R = \mathcal{R}/\mathcal{M}$$

$\mathcal{R}$ is the universal gas constant, and $\mathcal{M}$ the molecular weight of the mixture.

2. Transport Properties

Although the gas property parameters F and G require only the gas mixture viscosity, the viscous equations used here are valid only for a constant Prandtl number. For this reason, the thermal conductivity and the Prandtl number were calculated to check the behavior of the Prandtl number with a view toward selecting the gas mixture that best simulates testing in a nonequilibrium freestream. As a first step in analyzing the effects of a nonequilibrium freestream, it is assumed that the flow over a slender body in hypersonic, low density flow is frozen chemically and vibrationally within the boundary layer as well as in the inviscid flow field. There is experimental evidence from spectroscopic probing of the boundary layer in the nozzle of an arc tunnel[16] which supports this frozen flow assumption.

The transport property calculations are further simplified by considering only mixture properties at standard temperature and pressure (STP). Variations with temperature are assumed to be given in the form of the Sutherland relation, i.e., the parameters F and G are formed from a ratio of mixture properties to those of air at STP with the Sutherland temperature dependence for air implicitly included in the viscous equations. The approximation appears realistic based on the results of Ref. 17 which gives transport properties of air-helium mixtures up to a temperature of 2700°R.

For air-helium mixtures the transport properties were taken

from Ref. 17. A few check calculations indicate that these results are compatible with results obtained using the calculation procedure described below.

For air-argon mixtures and frozen dissociated air considered in this study, the transport properties were calculated using the semi-empirical equations[18] of Wilke for viscosity and of Mason and Saxena for conductivity. The viscosity and thermal conductivity are given by

$$\mu = \sum_i \mu_i \left[1 + \sum_{\substack{j \\ j \neq i}} G_{ij} \frac{\beta_j}{\beta_i} \right]^{-1} \tag{32}$$

$$k = \sum_i k_i \left[1 + 1.065 \sum_{\substack{i \\ j \neq i}} G_{ij} \frac{\beta_j}{\beta_i} \right]^{-1} \tag{33}$$

where the influence coefficients, G_{ij}, are

$$G_{ij} = \frac{1}{\sqrt{8}} \left(1 + \frac{\mathcal{M}_i}{\mathcal{M}_j} \right)^{-1/2} \left[1 + \left(\frac{\mu_i}{\mu_j} \right)^{1/2} \left(\frac{\mathcal{M}_j}{\mathcal{M}_i} \right)^{1/4} \right]^2 \tag{34}$$

and the summations are taken over all of the i and j species. The μ_i and k_i are the viscosity and thermal conductivity of each species as a pure gas, the β's are the mole fraction of each species, and the $\mathcal{M}_i$'s are the molecular weights of each.

Neglecting the formation of nitric oxide, the mole fraction for dissociated air is calculated from the molar balance relation

$$0.78\ N_2 + 0.21\ O_2 + 0.01\ Ar \rightarrow \left(0.78 - \frac{b_N}{2} \right) N_2 + b_N N + \left(0.21 - \frac{b_O}{2} \right) O_2 + b_O O + 0.01\ Ar \tag{35}$$

It is assumed that oxygen dissociation is completed before any appreciable nitrogen dissociation occurs so that up to a value of $\beta = 0.3$[47]

$$\beta = \beta_O = \frac{b_O}{1 + \frac{b_O}{2}}$$

and beyond this

$$\beta = \beta_{O+N} = \frac{0.42 + b_N}{1.21 + b_N/2}$$

For the air-argon mixtures the molar balance is

$$0.78\ N_2 + 0.21\ O_2 + 0.01\ Ar \rightarrow 0.78\ N_2 + 0.21\ O_2 + (0.01 + b_A)Ar \tag{36}$$

giving

$$\beta = \frac{b_A}{1 + b_A}$$

Except for the radicals O and N, the viscosities and thermal conductivities of each constituent were taken from Ref. 19 and are presented in Table I. As usual, some approximation to the properties of O and N are required. It is assumed that $\mu_O \approx \mu_{O_2}$, $\mu_N \approx \mu_{N_2}$, and $k_O = k_N = 1 \times 10^{-4}$ g/cm-sec. The values of k_O and k_N are intermediate to what one obtains by using the monatomic relation,

$$k_i = \frac{15}{4} \frac{\mathcal{R}}{\mathcal{M}_i} \mu_i \tag{37}$$

and values interpolated from the variation of measured values of k vs. $\mathcal{M}$ for inert monatomic gases.

The resulting influence coefficients, G_{i_j}, for all species considered here are presented in Table II.

Table I - Pure Species Properties at 300°K

	N_2	O_2	Ar	He
$\mu \times 10^7 \left(\frac{g}{cm\text{-}sec}\right)$	1786	2071	2270	1967
$k \times 10^7 \left(\frac{cal}{cm\text{-}sec\text{-}°K}\right)$	618	635	422	3719

Table II - Influence Coefficients, G_{ij}, Eq. 34

↓i \ j →	N_2	N	O_2	O	Ar	He
N_2		0.692	0.955	0.960	1.052	0.314
N	1.395		1.353	0.955	1.406	0.480
O_2	1.007	0.704		0.692	1.064	0.306
O	1.413	1.007	1.345		1.449	0.471
Ar	0.935	0.628	0.934	0.638		0.274
He	2.425	1.845	2.307	1.790	2.370	

3. Nonequilibrium Nozzle Expansions

A primary objective of this study was to develop techniques to allow test results from high-energy, nonequilibrium test facilities to be applied in the prediction of the performance of slender bodies in flight. In addition to the estimates of how a variable compsition or nonequilibrium free stream affects the inviscid and viscous flow on a slender body, we must have a reasonably accurate means of predicting the gas composition which results from a nonequilibrium expansion in a wind tunnel nozzle. For high energy air wind tunnels which operate at a high pressure, e.g., shock tunnels and high pressure arc tunnels, sizeable chemical and vibrational relaxation can occur downstream of the nozzle throat. Under these conditions Refs. 20-22 show that the frozen gas composition correlates quite closely with reservoir entropy. In Ref. 23 a more comprehensive parameter is developed which includes the geometrical

parameters of the nozzle in addition to the reservoir entropy. The limitations of the results of Ref. 23 are pointed out in Ref. 24 where it is shown that the approximation breaks down for enthalpies such that $T_o > 8000°K$ (conditions beyond the capabilities of most high energy wind tunnels).

For low pressure arc wind tunnels, such as that used in these studies, the assumption that the vibrational and chemical relaxation region is located appreciably downstream of the throat is no longer valid and the simple assumption that the flow freezes at the nozzle throat is more appropriate. The detailed analysis of the OSU arc tunnel[16] which operates at a reservoir pressure near 1 atmosphere shows that the test section properties are very nearly those which would result from flow-freezing at the throat.

4. Analytical Results

The results of the calculations of the Prandtl number, the boundary layer displacement thickness parameters, F, the skin-friction and heat transfer parameter, G, and the ratio of specific heats are presented in Figs. 1a-d. It is to be noted that the departure of the viscous parameters F and G for air-helium mixtures from those for frozen dissociated air are almost negligible for atomic mole fractions up to values corresponding to the complete dissociation of oxygen. However, because of the low molecular weight of helium, the Prandtl number for air-helium mixtures varies greatly from that for frozen dissociated air while that for air-argon mixtures remains quite close to that of air. It was this feature that resulted in the choice of air-argon mixtures for the present tests. In passing, we note that other combinations were considered and discarded: the optimum binary mixture of neon and air appears to be prohibitively costly for an extensive wind tunnel test program, while a ternary mixture of argon, helium and air that can be tailored to match the thermodynamic properties of frozen, dissociated air exhibits the same type of variation in Prandtl number as shown in Fig. 1a.

The atomic mole fractions, β, for a nonequilibrium expansion of high temperature air are shown in Fig. 2. Flow freezing at the throat was assumed and calculations were conducted at reservoir entropies and pressures characteristic of the arc tunnel conditions of the present tests. For comparison, we include from Ref. 23 the mole fractions for the geometry of the OSU arc tunnel for a high pressure expansion where the relaxation region is located downstream of the throat. In this case the relaxation region or effective point of freezing moves downstream as pressure is increased such that the test section gas composition is a function of the reservoir entropy alone for a fixed nozzle geometry. As pressure is increased at constant entropy the test section dissociation level approaches a limit given by the dashed curve labeled "entropy correlation." At a reservoir pressure of 1 atmosphere, which is in the range covered by the present tests, the assumption that the flow freezes

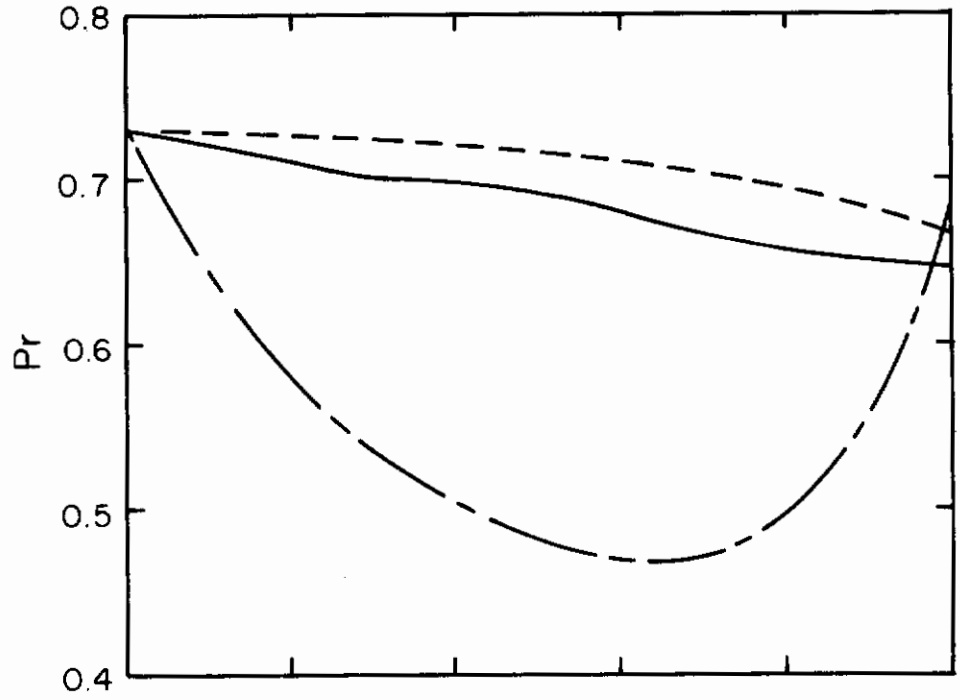

a. Prandtl Number

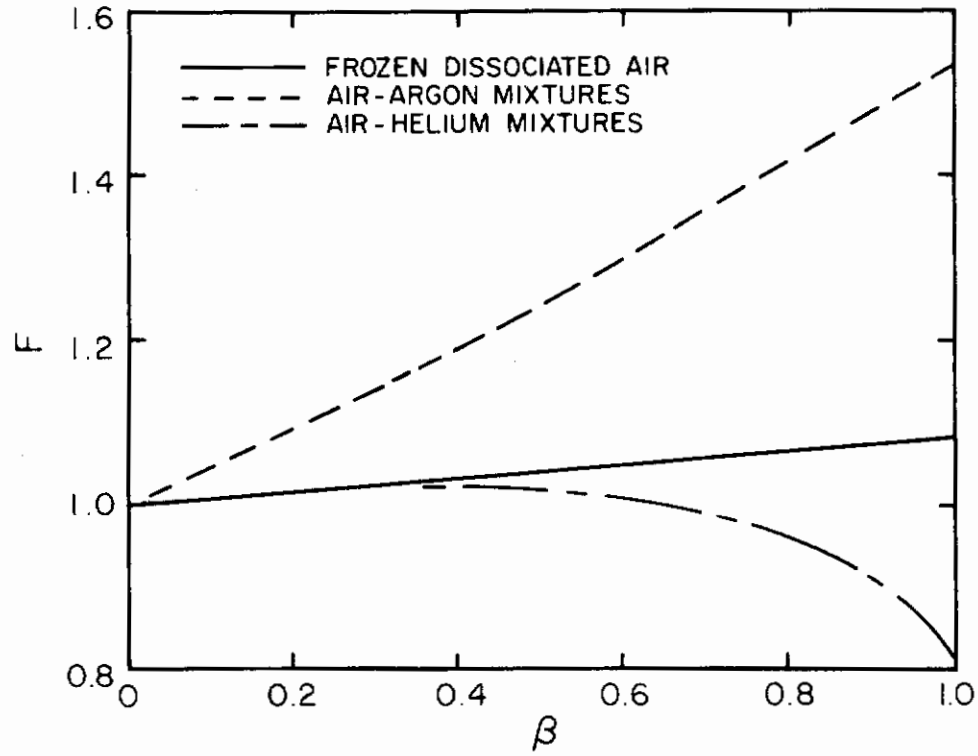

b. Boundary Layer Growth Parameter

Fig. 1 - Gas Property Parameters for Frozen Dissociated Air, Air-Argon Mixtures and Air-Helium Mixtures

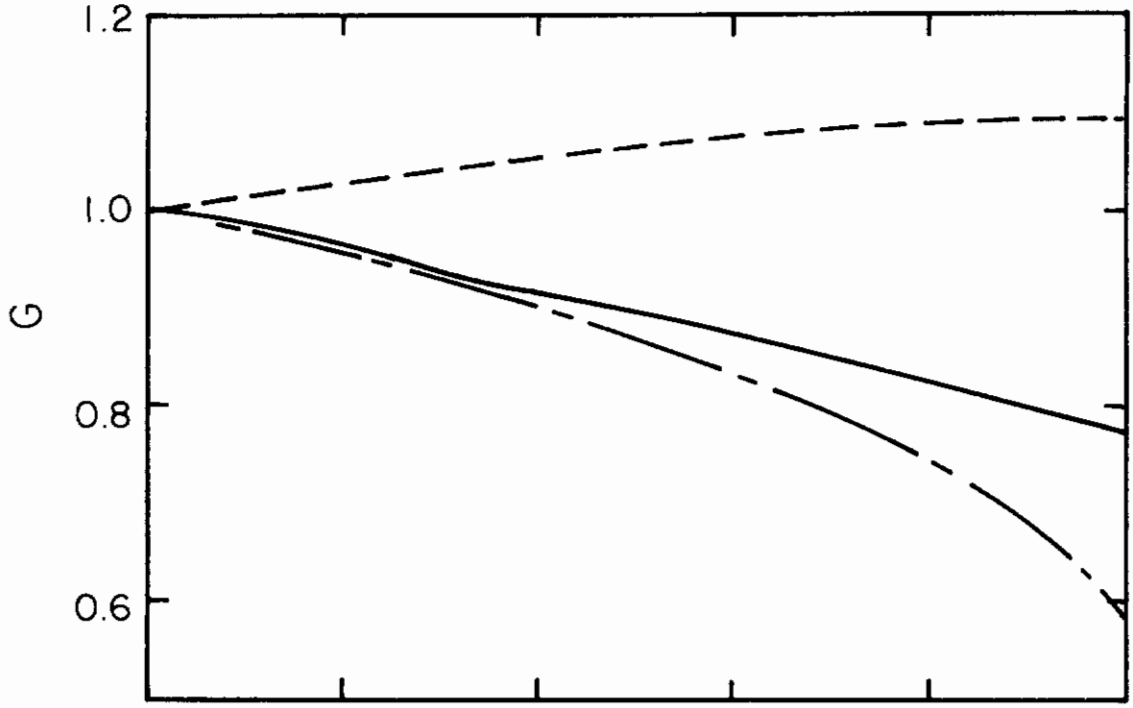

c. Skin-Friction and Heat Transfer Parameter

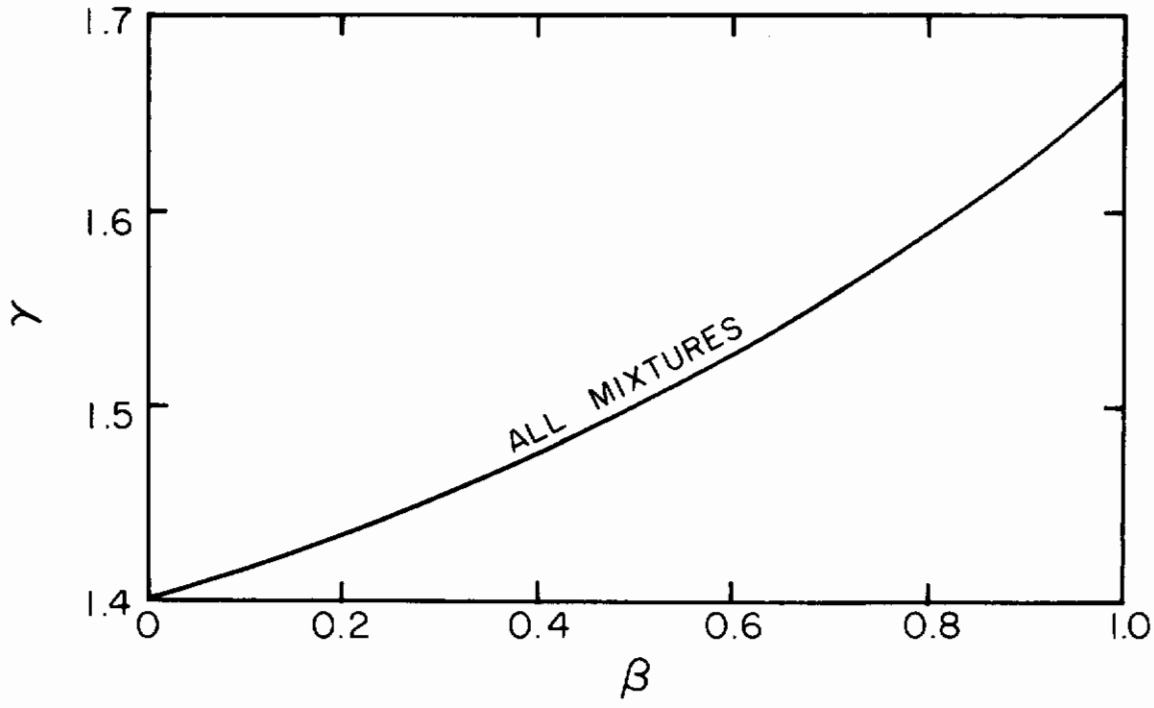

d. Freestream Ratio of Specific Heats

Fig. 1 - Continued

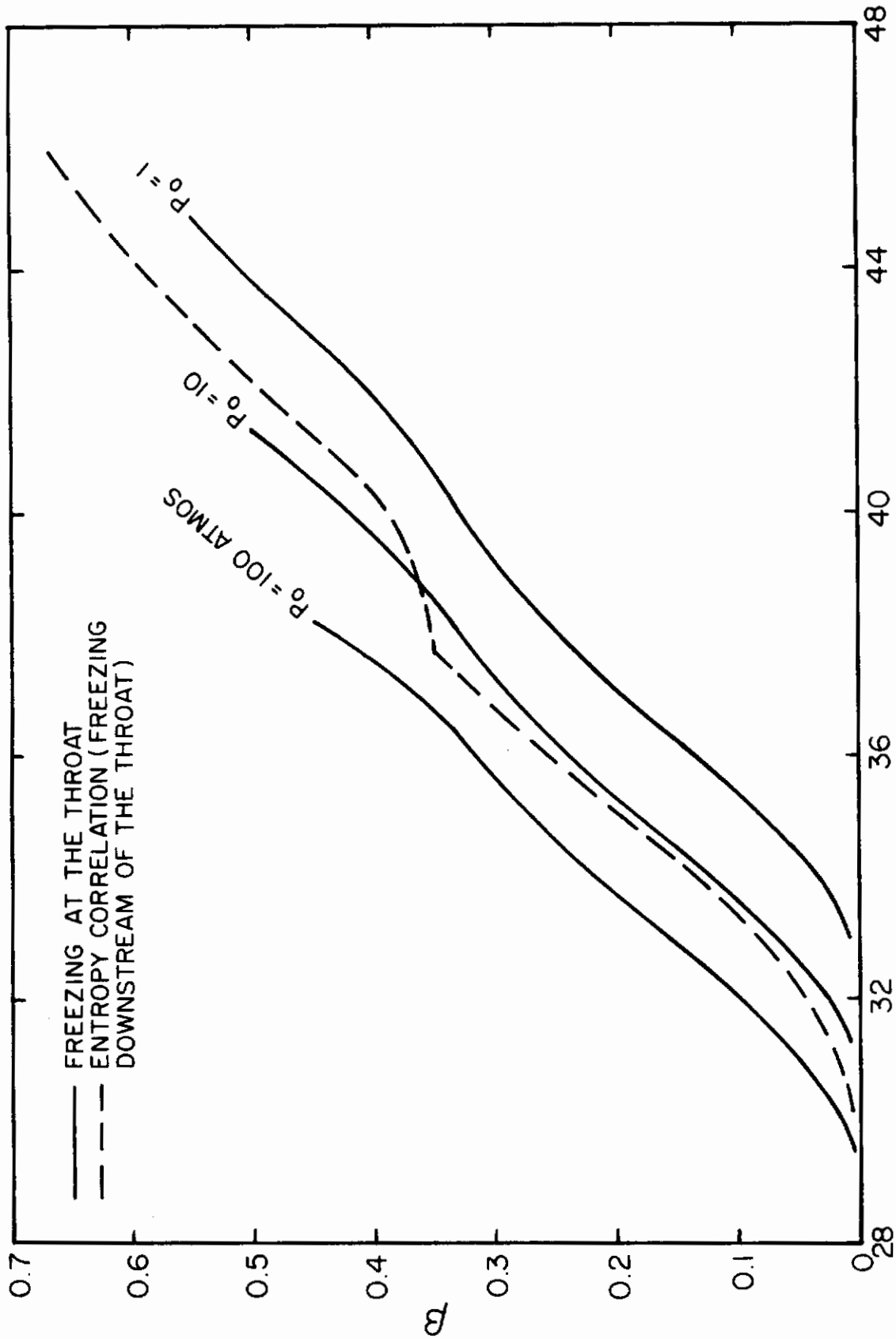

Fig. 2 - Test Section Atomic Mole Fraction for Nonequilibrium Air Expansions

at equilibrium throat conditions is realistic; at 100 atmospheres this same assumption over estimated the dissociation level; the overlapping of the two results in the neighborhood of 10 atmospheres suggest that it is in this range that the effective point of freezing proceeds to move downstream from the throat.

III. EXPERIMENTAL

Experimental pressure and heat transfer studies were performed in both arc-heated and perfect-gas, variable-atmosphere wind tunnels. The objective of these tests was to evaluate the effects of variable composition and nonequilibrium freestreams on simple shapes such as sharp flat plates and cones.

A. TEST FACILITIES

The variable atmosphere studies were conducted in the OSU 12-inch hypersonic wind tunnel with a contoured nozzle operating at a nominal Mach number of 10. This facility is driven by an electrical resistance heater which provides air stagnation temperatures up to 2400°F at pressures up to 2600 psia on a continuous basis. For these studies, reservoir pressures in the range $50 \leq P_o \leq 150$ psia were employed. Air-argon mixture ratios were established by choked air and argon control valves while the wind tunnel nozzle also remained choked and the tunnel reservoir temperature was automatically controlled at a value of 1400°F. The wind tunnel was started by manually presetting a reduced reservoir pressure and, after stabilization, by introducing argon to attain the desired reservoir pressure. The mixture ratio can be calculated accurately from the measured initial air pressure and the final mixture pressure. The starting procedure was reversed after completion of the test run to ensure that the air flow rate was not affected by depletion of the air storage tanks. Because of the relatively small amount of air consumed in these low pressure tests, the final air-only pressure showed no observable change from its initial value. Complete mixing of the two gas streams was assumed since the wind tunnel heater provides a nearly ideal mixing chamber. The gases are introduced into the heater regeneratively to cool the outer shell and this results in nearly 100% utilization of the electrical power. Heating proceeds by passing the gas through a series of 76 resistor grids. In addition to the heating grids, there are turbulence grids located within the heater channel. This configuration ensures that the gases are well mixed by the time they reach the nozzle entrance.

The OSU arc-heated wind tunnel consists of an air arc heater, settling chamber, a 7-$\frac{1}{2}$° half-angle conical nozzle with a 4-inch diameter exit, a free jet test cabin, diffuser and vacuum system. The arc heater

is a direct current type with cylindrical electrodes upstream and downstream of a central air injector. The arc column is vortex stabilized and uses a magnetic spin coil on the rear electrode (cathode). For these tests the arc heater was operated at a pressure close to 1 atmosphere and enthalpies between 3000 and 4000 Btu/lb_m.

B. TUNNEL CALIBRATIONS

The basic measurements which determine the test section flow properties in the 12-inch hypersonic wind tunnel are the reservoir pressure measured with a Bourdon-tube gage, the reservoir temperature measured with a platinum-platinum rhodium thermocouple located at the exit of the resistance heater, and detailed surveys of the test section pitot pressure. The pitot-to-reservoir pressure ratio is used to determine the Mach number and p_∞ assuming an isentropic expansion for a specified γ. The freestream dynamic pressure is given quite accurately by

$$q_\infty = \frac{\gamma + 1}{\gamma + 3} p_{t_2} \tag{38}$$

where p_{t_2} is the measured pitot pressure. This approximation is derived from the normal shock momentum equation and the constant density Bernoulli equation for the post-shock flow which eventually stagnates at the pitot probe. It is accurate to within 1% for Mach numbers as low as 7 and has the advantage that the effect of variations in atmospheric composition, throught γ, is simple and explicit. Radial surveys of the pitot pressure distributions were obtained throughout the complete range of reservoir pressures and gas mixtures employed in this series of tests. Off-center pitot pressure was monitored simultaneously with model data and this was related to the pitot pressure at the model location from the radial survey data.

To estimate the arc tunnel reservoir temperature or enthalpy some method other than a direct thermocouple measurement must be employed. In this case, in addition to the standard reservoir and pitot pressure measurements, the mass flow rate of air to the heater is measured and the reservoir enthalpy is calculated using the equilibrium-sonic-flow (ESF) method. That is, if the enthalpy is uniform it is uniquely related to the measured mass flow, throat size, and measured reservoir pressure assuming that the gas is in thermo-chemical equilibrium up to the throat. While the ESF method has met with varying degrees of success it appears to be accurate for the configuration and operating conditions of the OSU arc tunnel.[16]

Under the assumption that the flow is frozen in the rapid expansion downstream of the throat, the test section Mach number and p_∞ may be estimated from an isentropic expansion with γ equal to the throat value.

An additional calibration is performed in the arc tunnel with a mass flux probe. This measurement together with the pitot pressure gives a method of estimating the freestream density and velocity. For a sample case, the directed energy obtained from this velocity estimate added to the sum of the energy frozen in at the throat and the estimated free-stream static enthalpy gave a total enthalpy only 1% lower than the ESF method. Although this accuracy in calibrating an arc tunnel is not necessarily typical, the sample calculation suggests that reasonable estimates of freestream flow properties can be otained. Previous checks on the methods used to define the arc wind tunnel operating conditions (Ref. 16) have employed spectroscopic analysis of the test section flow as well as a total energy balance comparison. All of these checks are consistent with the assumptions that the flow is uniform and in equilibrium up to the throat and that the flow is frozen in chemical composition in its further expansion downstream of the throat.

C. MODELS

Three sharp flat plate models and three cone models were used. For the variable atmosphere studies in the 12-inch hypersonic wind tunnel, the flat plate pressure and heat transfer models were approximately 2.5 inches in chord and 8 inches in span and supported by a spanwise sting. These models spanned the free-jet test core of approximately 5 inches in diameter to minimize end effects. The water cooled pressure model contained spanwise sets of three 0.030-inch diameter orifices at five axial stations. The stainless steel heat transfer model contained a central instumentation panel 0.010-inch thick with copper-constantan thermocouples welded to the under side at seven axial stations. Both of these models were beveled at 30° on the under side of the leading edge. The third model tested in the 12-inch tunnel was a 10° half-angle cone heat transfer model. As opposed to the thin-skin model used for the flat plate test, this cone model was constructed of black teflon and the heating rates were determined by the melting of a phase-change coating. Previous data obtained with this technique on blunted cones (Ref. 25) correlated quite well with transient thin skin measurements. The 4.6-inch long teflon cone model had a brass tip forward of the 1/8-inch diameter station to ensure the integrity of the sharp tip and the absence of bluntness effects caused by tip ablation.

For the arc tunnel tests, cone heat transfer was measured with phase change coatings on a 10° half-angle cone which was one-half the size of that used in the 12-inch tunnel. A water-cooled cone pressure model of the same scale as the teflon heat transfer model was also tested in the arc tunnel. Finally, a teflon sharp plate with phase change coatings was tested in the arc tunnel. This model, with a 20° leading edge bevel, was tested with both teflon and brass edges.

D. DATA ANALYSIS

Wind tunnel corrections to data obtained in the 12-inch hypersonic tunnel were minimal because of the flow uniformity obtained with the contoured nozzle. Some care was taken to ensure that the flow properties at the model location were properly corrected for variations in reservoir pressure and the gas mixture.

The arc tunnel employed a conical nozzle and the model dimensions were not negligibly small compared to the core diameter. Hence, source flow effects were considered. These effects were particularly severe for the cone model where flow angularity as well as the axial centerline variation of flow properties had to be considered. To correct for source flow effects, the local flow properties were employed to reduce the data, e.g., local values of q_∞, $\rho_\infty u_\infty$ and p_∞ . To correct off-centerline data, the calculated angularity of the flow was added to the local model inclination angle. This provides an estimate of the flow deflection that would be obtained in the absence of source flow effects.

Thermomolecular corrections to measured model pressures were small. Because all pressures were measured on water-cooled models where the temperature was not significantly greater than the temperature of the external pressure transducer, thermal transpiration effects were negligible. Orifice effects are most pronounced for the cone pressure tests in the arc tunnel and these, according to Ref. 26, amount to a 2 to 4% correction. Since this correction is within the scatter of the data upon which the semi-empirical correction estimates of Ref. 26 are based, and an order of magnitude less than the total source flow correction, the orifice effect correction was neglected.

The heat transfer experiments covered a wide range of energy levels. The variable atmosphere studies were at conditions where it is appropriate to define the Stanton number in the usual way,

$$St = \dot{q}/\rho_\infty u_\infty c_p (T_{aw} - T_w) \tag{39}$$

The arc tunnel data and the comparative shock tunnel results are at energy levels where adiabatic wall conditions are far beyond material capabilities and hence, the true adiabatic wall temperature cannot be verified experimentally. In this case, it has become customary to use a heat transfer rate coefficient in the form

$$C_H = \dot{q}/\rho_\infty u_\infty (H_o - H_w) \tag{40}$$

where the heating rate is assumed proportional to the difference between the total enthalpy and the enthalpy of the gas at the wall temperature. This definition of heat transfer rate coefficient is not compatible

with the Stanton number at lower energy levels. For comparing a wide range of data a choice of heat transfer parameter must be made. That is, either the latter definition of C_H must be used or the Stanton number can be employed by extending the concept of an adiabatic wall and defining

$$St = \dot{q}/\rho_\infty u_\infty (H_{aw} - H_w) \tag{41}$$

We choose here the use of the heat transfer rate coefficient as given in Eq. (40).

Since the transient thin-skin heat transfer measurement technique is reasonably straightforward, the remaining data analysis method worthy of note is that for reducing the phase change coating data to heat transfer rates. In Ref. 25 the solution for the semi-infinite plate with time dependent heat transfer rate was applied successfully for the determination of heat transfer rates on blunted cones. For the present tests with sharp cones where the penetration depth of the heat pulse may not always be negligibly small compared to the body radius, the one-dimensional approximation used in Ref. 25 is no longer valid. The equation developed and used in this study employs linearized corrections of both the time dependence of the heat transfer rate, and the radial effect for axisymmetric bodies and is

$$\dot{q} = \frac{\sqrt{\pi}}{2}\sqrt{k\ell\rho}\,\frac{T_p - T_i}{\sqrt{t}}\left[1 + \frac{\sqrt{\pi}}{2}\Theta - 1.46\tau\right] \tag{42}$$

where the model material properties are

k = thermal conductivity

ℓ = specific heat

ρ = density

α = thermal diffusivity.

T_p is the melting temperature of the phase change coating, T_i the initial temperature of the model surface and t the time to melt, or the time for the surface temperature to increase from T_i to T_p. The leading term in this equation is simply the solution for a semi-infinite plate with a constant heat transfer rate applied at t = 0. The second term is the

correction for the reduction in heating rate as the surface temperature increases, where $\Theta = (T_p - T_i)/(T_{aw} - T_w)$, and the third term is the correction for radial effects where $\tau = \alpha t/r^2$ and r is the local radius of the axisymmetric body. Figure 3 shows the heating rate to a teflon cone for a typical run in the 12-inch hypersonic wind tunnel where Eq. (42) was used for data reduction. Also shown are the heating rates that one would calculate by successively neglecting the radial correction and then the time dependent heat transfer rate correction.

IV. EXPERIMENTAL RESULTS AND DISCUSSIONS

A. PRESSURE STUDIES

The measurements of surface pressure on a sharp flat plate for air and air-argon mixtures obtained in the 12-inch hypersonic tunnel are summarized in Fig. 4. For angles of attack on the windward surface of 0°, 5°, and 10° the mole fraction of argon additive varied from $\beta = 0$ to 0.33. The maximum β-value is approximately equal to the atomic mole fraction for nonequilibrium air with complete oxygen dissociation. In these tests, the gas property parameter F varies from unity for air to $F = 1.152$ for $\beta = 0.33$; x^*/x is as high as 0.716 for the high pressures at $\alpha = 0°$ and as low as 0.677 toward the leading edge at $\alpha = 10°$; T_w/T_o is very nearly a constant at 0.315. The predictions of Eqs. (2) and (12) for $\alpha = 5$ and 10° and Eq. (20) for $\alpha = 0°$ are shown by the solid lines for $\gamma = 1.4$ and the dot-dashed lines for $\gamma = 1.46$. These were the limits of the γ variation. The Mach number used to estimate p_∞/q_∞ was obtained for an isentropic expansion at each value of γ. Thus, for air the Mach number is 9.8 and for an air-argon mixture with $\beta = 0.33$, the Mach number is 11.3.

The most notable feature of Fig. 4 is that Eqs. (2), (12) and (20) predict the pressure coefficient quite accurately. Theoretical prediction was not the primary purpose of the analysis; rather the goal was to reflect the influences of variable gas properties on the surface pressure, and, in this case where T_w/T_o is nearly constant, to demonstrate the applicability of the simplified rarefaction parameter $(\rho_\infty x^*)^{-1/2}$. The departure of the data from the analytical prediction is generally accepted to result from the onset of the merged-layer regime. The point of departure depends largely on the value of T_w/T_o. Here the departure occurs in the range of the rarefaction parameter of Fig. 4 between 6000 and 8000.

It should also be noted from Fig. 4 that the gas property parameter, F, is required to obtain correlation of the data.

Finally, from Fig. 4 we can observe that, at least for this small range of Mach number, the viscous induced pressure at a point on a sharp

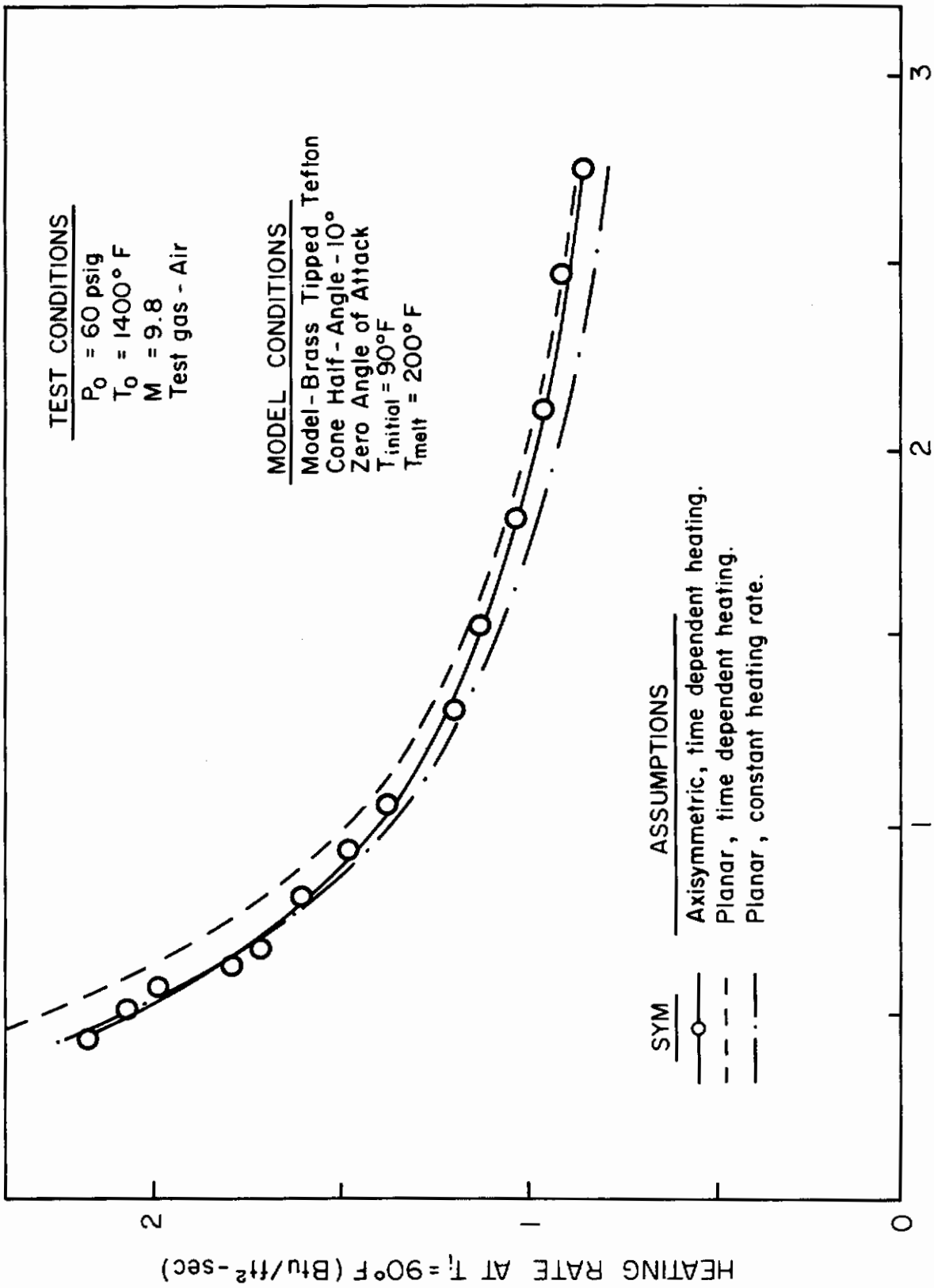

Fig. 3 - Sharp-Cone Heat Transfer Rates Using Phase Change Coatings

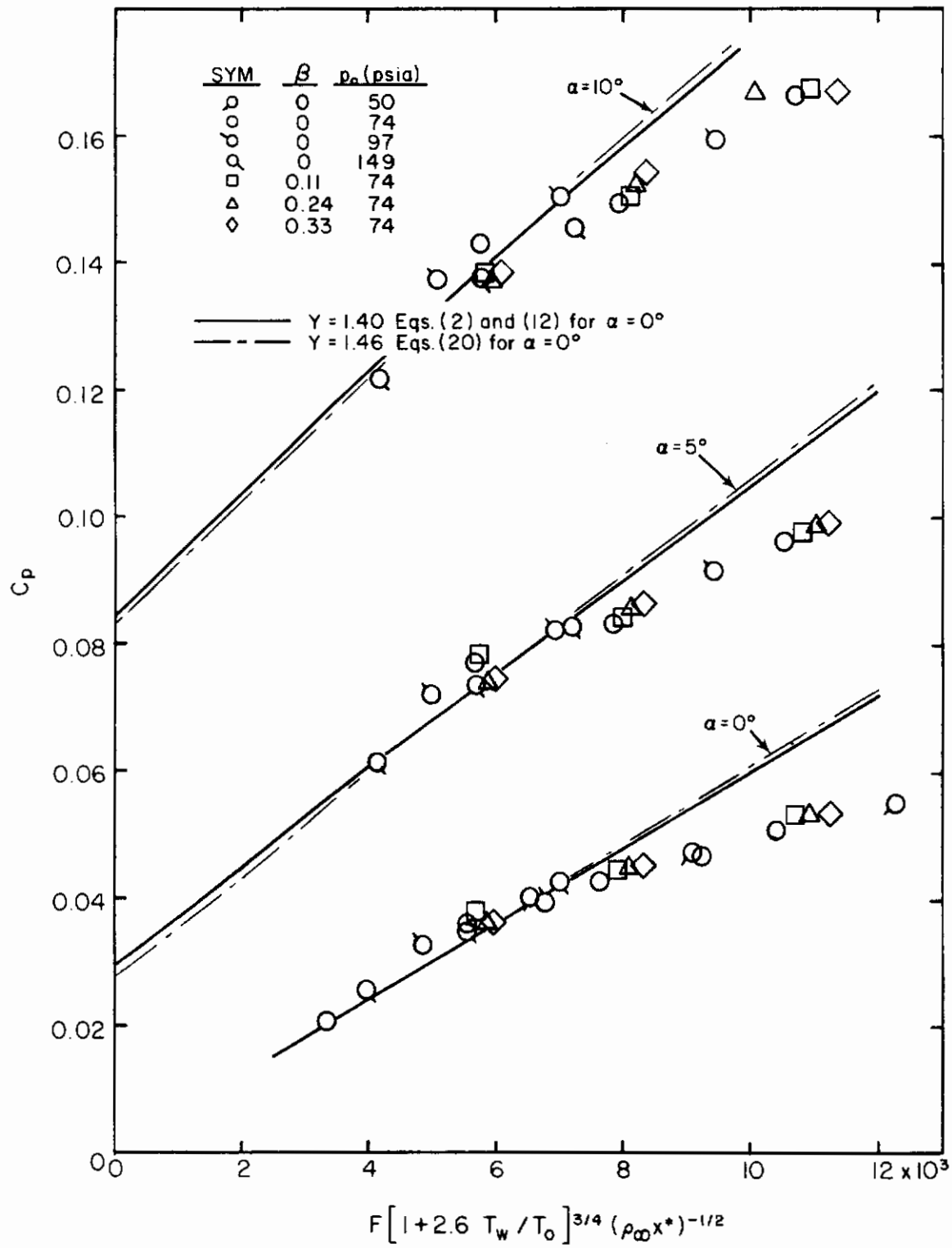

Fig. 4 - Surface Pressure Coefficient on a Sharp Flat Plate in Argon-Air Mixtures

inclined plate for a given atmospheric composition and at a given wall temperature ratio is a unique function of the freestream density.

Although the Mach number range of Fig. 4 is too small to evaluate Mach number effects, the minimal dependence of viscous interaction pressure on Mach number has been demonstrated in Ref. 13 and is further emphasized in Fig. 5. This Mach number independence results from the manner in which the similarity parameters are formulated. In Fig. 5, the present variable-atmosphere results at zero angle of attack are compared with Kendall's[27] data at M = 5.8 in air and Feldhuhn's[28] results at M = 16.3 in helium. The variables which make up the similarity parameter in Fig. 5 vary widely and the only significant divergence in the correlation is that associated with the onset of merging (due to the differences in T_w/T_o). Because we can use the explicit expression for C_p for $\alpha = 0°$, all of the effects of a variable γ may be combined. Thus, the rarefaction parameter used in Fig. 5 differs from that of Fig. 4 by the factor $[(\gamma + 1)/2.4]^{½}$. Variations in the gas property parameter, F, span a range from 0.866 for the helium data to 1.168 for the air-argon mixture of $\beta = 0.331$.

Surface pressures on a sharp 10° half-angle cone also were obtained in the OSU arc tunnel. The results are shown in Fig. 6 where the measured surface pressure coefficient, corrected for source flow effects, is plotted against the physical surface coordinate. The data shows an apparent overexpansion of the type observed on blunted cones. However, the validity of the overexpansion is left open to question because the source flow corrections applied were large (of the order of 50%) and because the surface temperature distribution is not known in detail.

B. HEAT TRANSFER STUDIES

Heat transfer tests were performed on sharp flat plates and 10°-cones in both the 12-inch hypersonic tunnel and the 4-inch arc tunnel. The results of the variable atmosphere tests on a sharp plate in the 12-inch hypersonic tunnel are presented in Fig. 7 for angles of attack of 0°, 5° and 10°. A comparison of a plot of this same data neglecting the variation of gas properties reflected by the parameter G (not shown) indicates that although the variation of G is small it should be employed to obtain the best data correlation. The effect of variable mixtures on skin friction and heat transfer is small compared to that on induced pressure. The maximum value of G (for $\beta = 0.349$) causes only a 5% change in C_H.

Using the measured surface pressures, the data of Fig. 7 are reduced to the form of Eq. (13) and are shown in Fig. 8. The curves of Fig. 8 correspond to the averages through the data of Fig. 7. Considering the data scatter, it appears that the increase in heat transfer rate with angle of attack is associated almost entirely with the increase in surface pressure (as predicted by Eq. 13). The only consistent

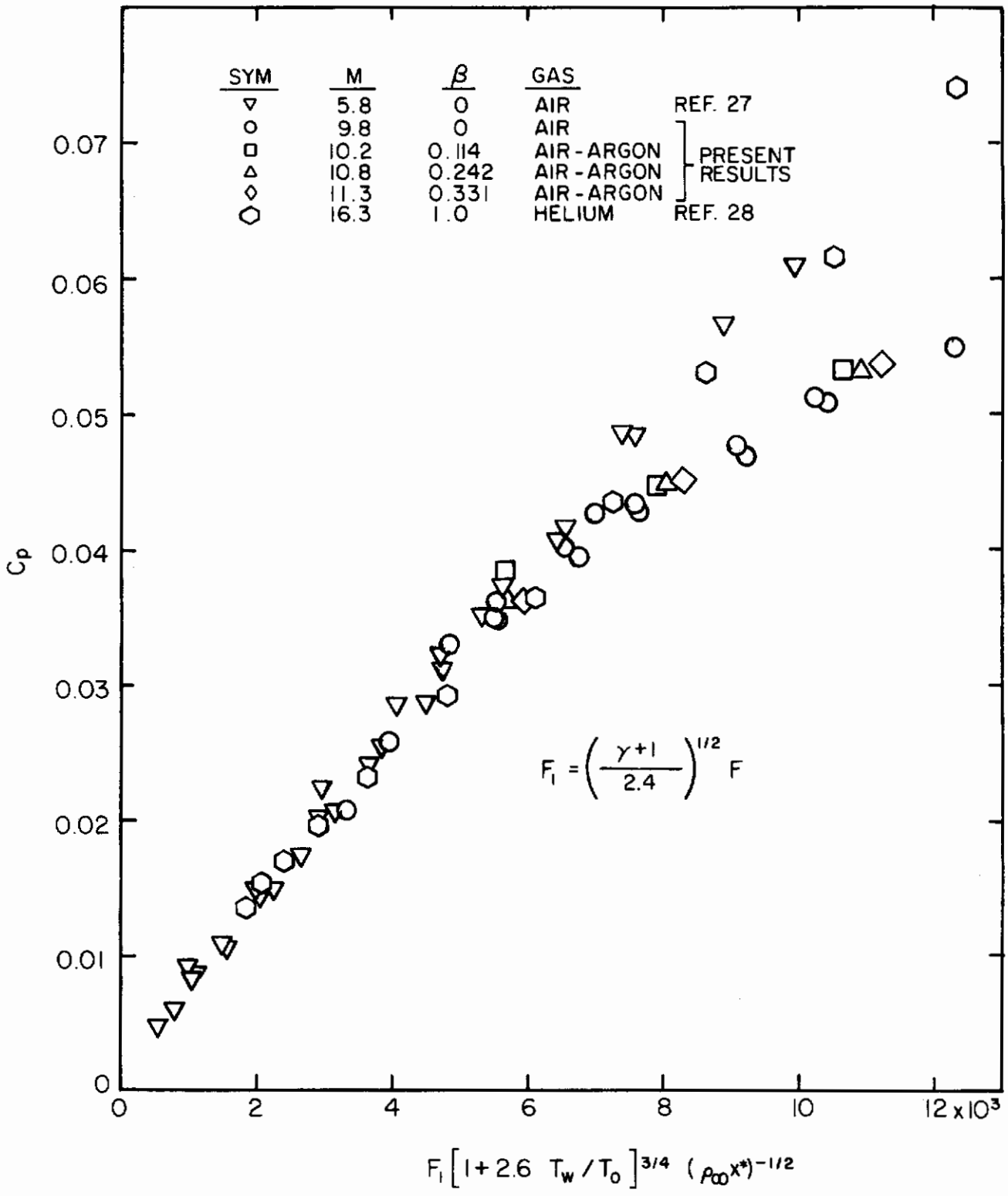

Fig. 5 - Viscous Induced Pressure Coefficient on a Sharp Flat Plate at Zero Angle of Attack in Variable Atmospheres

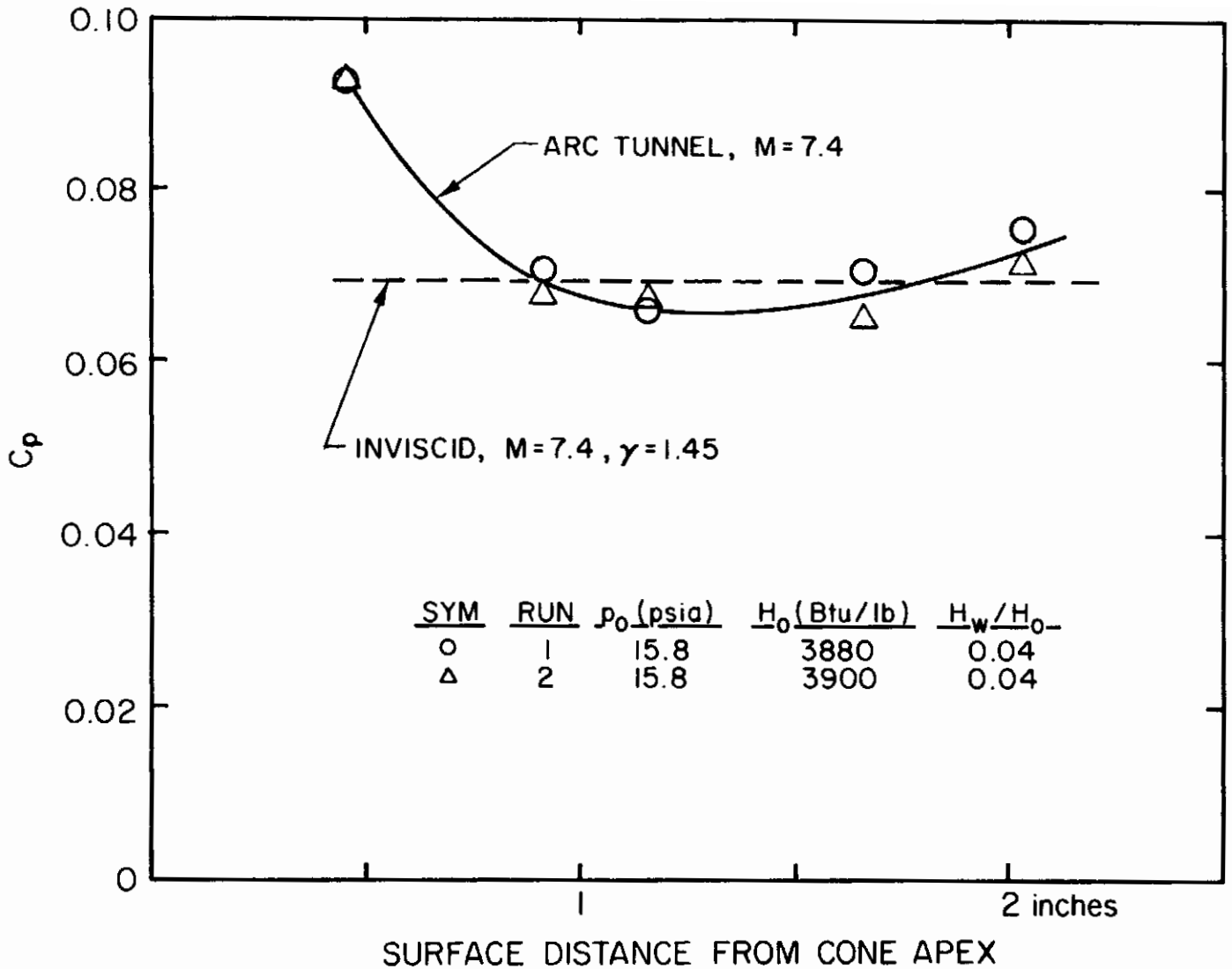

Fig. 6 - Surface Pressure Coefficient on a 10°-Half Angle Cone in a Low Pressure Arc Tunnel

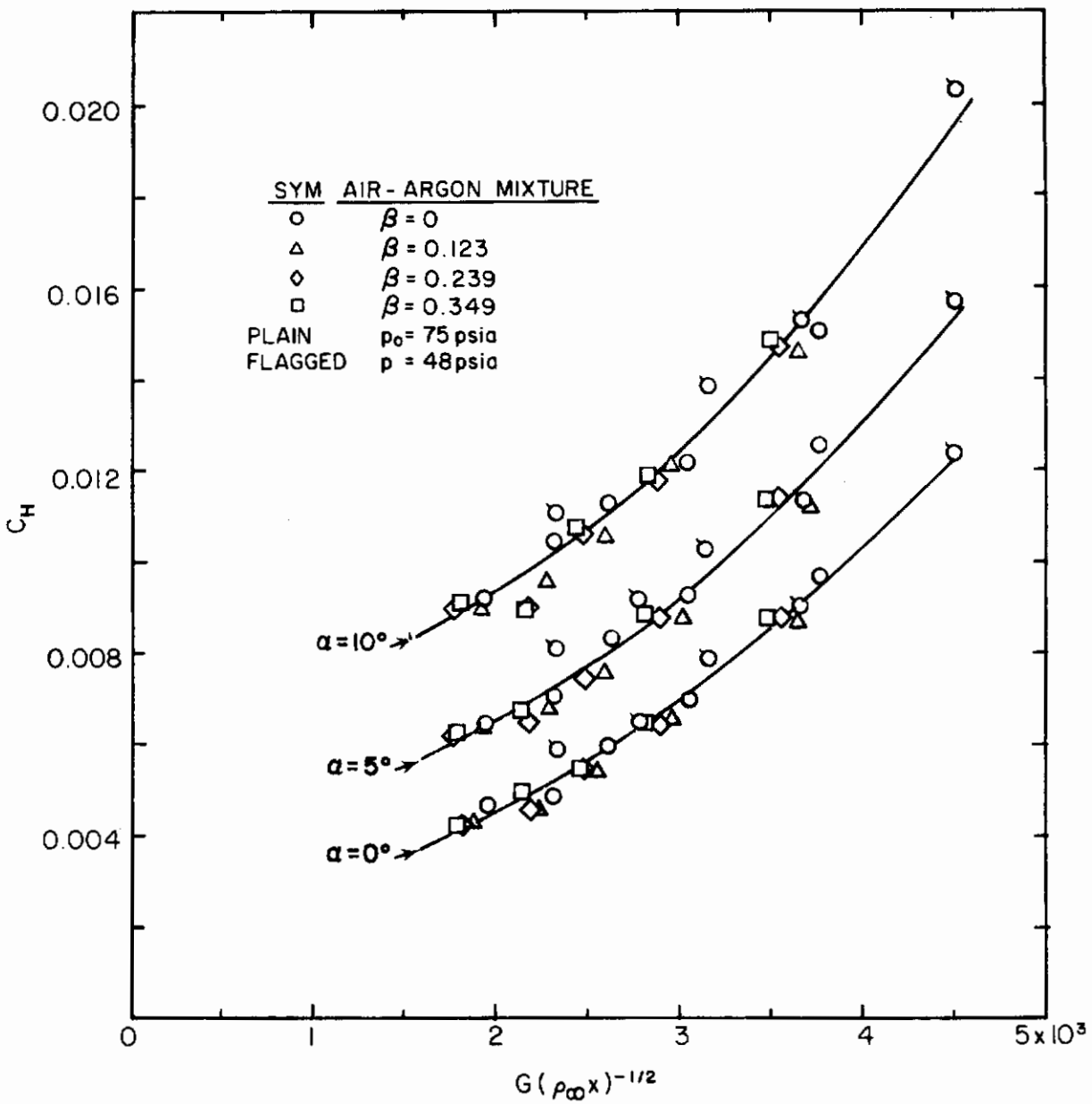

Fig. 7 - Heat Transfer Rate Coefficient on a Sharp Flat Plate in Air-Argon Mixtures

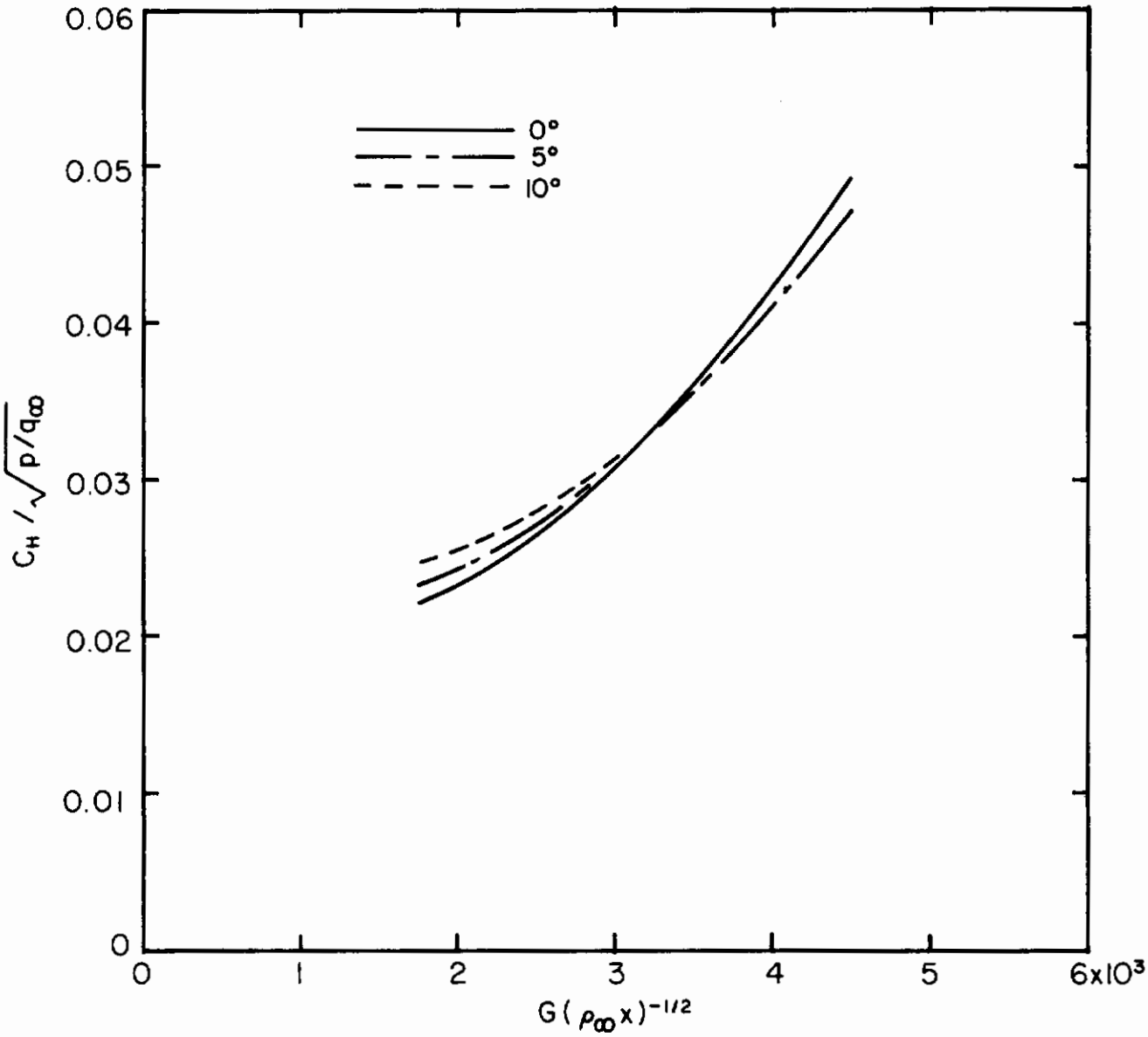

Fig. 8 - Reduced Heat Transfer Rate Coefficient on a Sharp Flat Plate in Air-Argon Mixtures

variation shown in Fig. 8 is an increase in $C_H/\sqrt{p/q_\infty}$ with angle of attack toward the trailing edge. This could result from flow nonuniformities since the model was pitched about a center of rotation located at the leading edge of the plate.

While the flat plate data in variable atmospheres was measured with a thin-skinned model, that for a 10°-half angle cone used phase change coatings on a teflon model. These latter results are shown in Fig. 9. All of these data were obtained by measuring the time to-melt for a paint having a melting temperature of 200°F. For a given test run the spread of the data is quite small. The primary experimental variabilitv is a run-to-run variation. Factors which influence this variability are differences in the calculated test conditions for different runs, the estimation of initial surface temperature based on subsurface measurements, and the effect of photographic lighting, coating thickness, and uniformity on the visual interpretation of the data. However, the overall spread of the data is similar to that for the transient-temperature, thin-skin technique.

The phase-change coating technique was first evaluated in the 12-inch hypersonic tunnel in the hope that this method would be effective in arc tunnels where previous experiments with thermocouples were unsuccessful because of electrical noise. Results of the phase-change coating test on a flat plate in the arc tunnel are shown in Fig. 10. One run was made with a teflon leading edge and two with a brass leading edge. All of the data were obtained by measuring the time for a 300°F paint to melt. The teflon leading edge ablated approximately 0.03 inch, although the edge remained sharp during ablation. As would be expected, the heat transfer rate was reduced under the influence of leading edge ablation.

Heat transfer to a 10°-half angle cone was also obtained in the arc tunnel using a brass-tipped teflon model and a 300°F melting point coating. The reduced data are shown in Fig. 11. Included for comparison is the 10°-cone phase-change coating data obtained in the 12-inch hypersonic tunnel with air-argon mixtures.

C. EXPERIMENTAL HEAT TRANSFER COMPARISONS

A wide variety of heat transfer results may be correlated with Eqs. (6) and (11). That is, we have the relation

$$\frac{C_H}{\sqrt{3^j p/q_\infty}} = \text{fn}\left[G(\rho_\infty x)^{-1/3}\right] \tag{43}$$

where $j = 0$ for a flat plate and $j = 1$ for a cone. A number of experiments on sharp plates and cones where pressure and heat transfer have

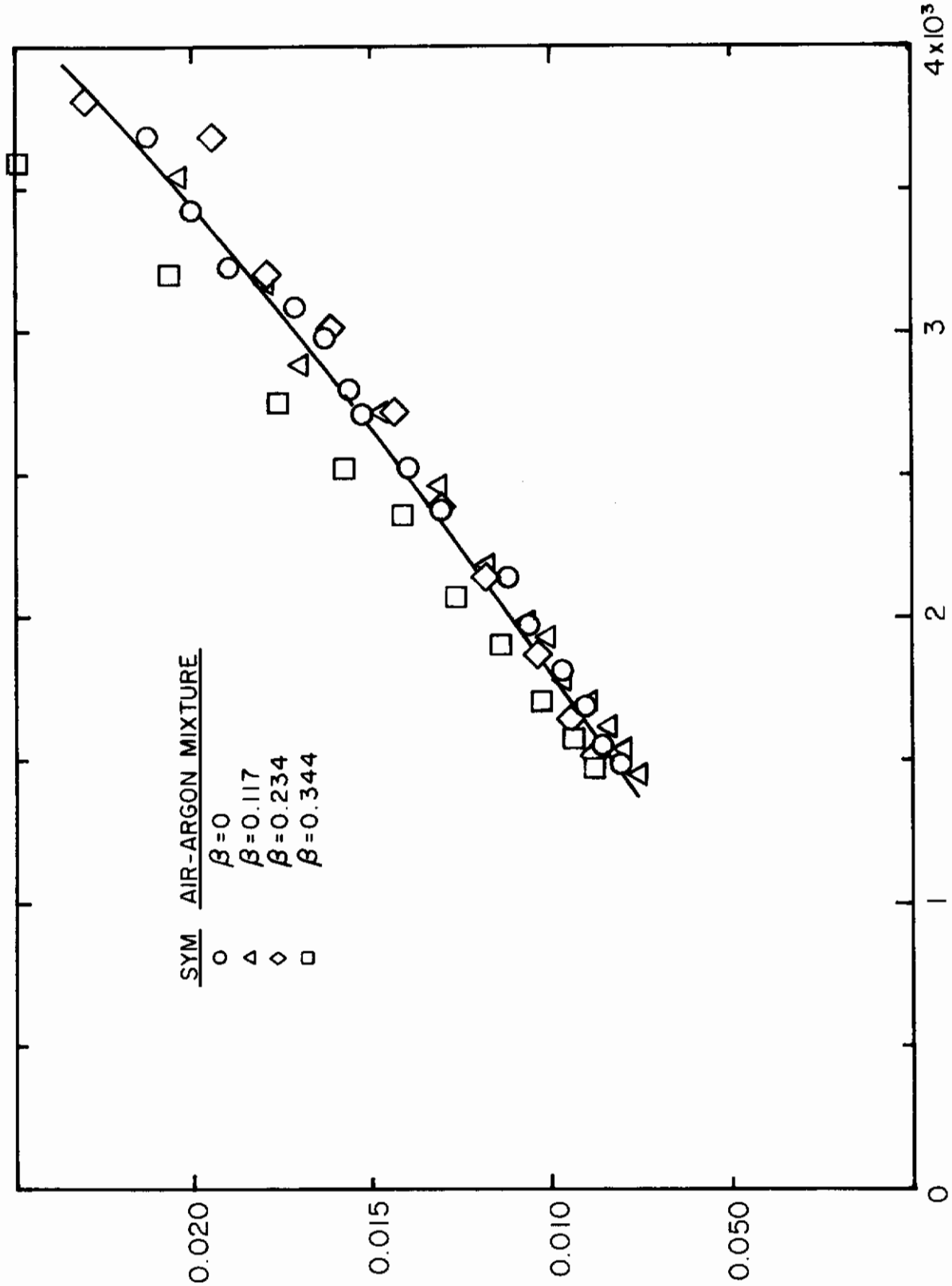

Fig. 9 - Heat Transfer Rate Coefficient on a 10°-Half Angle Cone in Air-Argon Mixtures

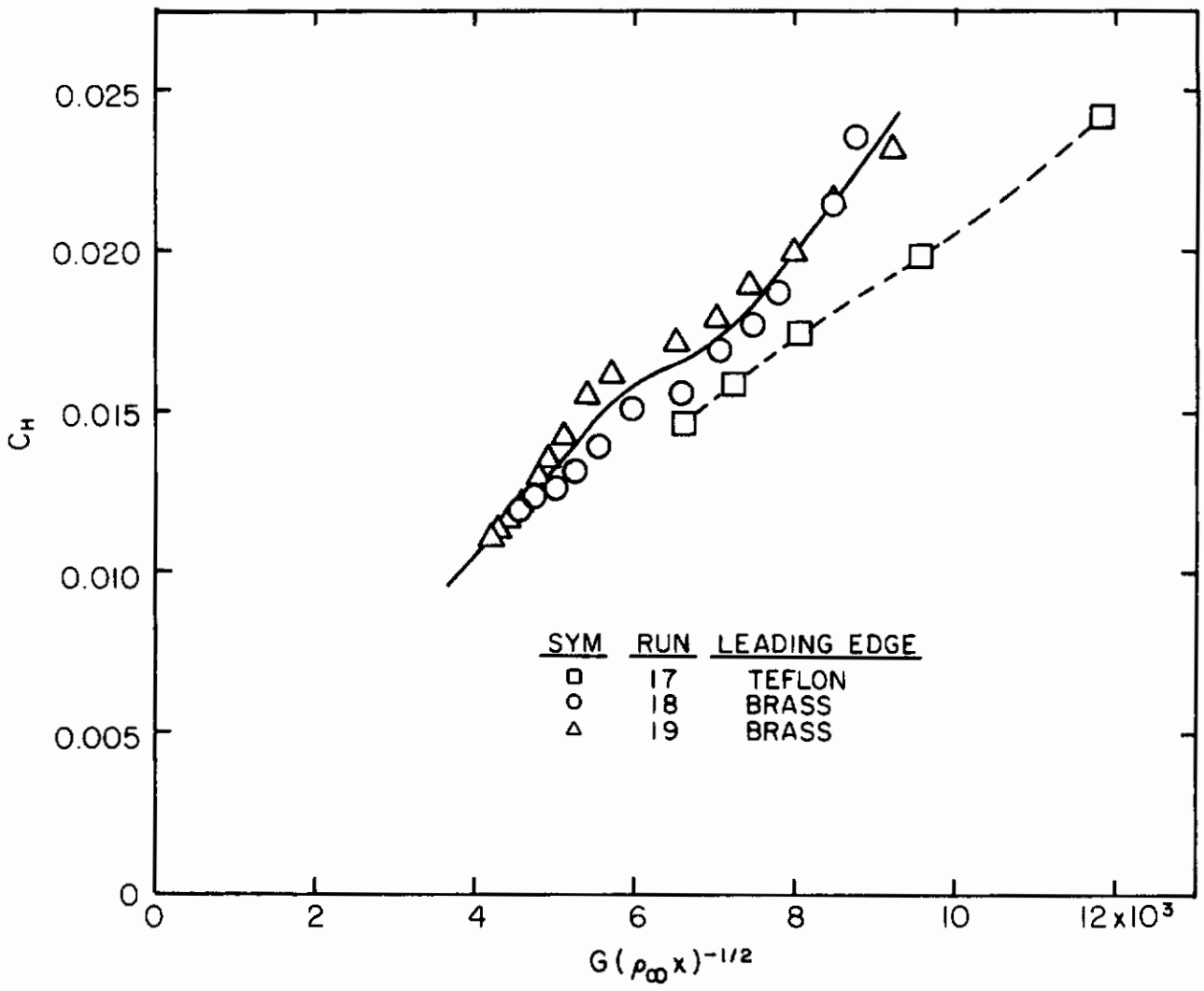

Fig. 10 - Heat Transfer Rate Coefficient on a Sharp Flat Plate at Zero Angle of Attack in a Low Pressure Arc Tunnel

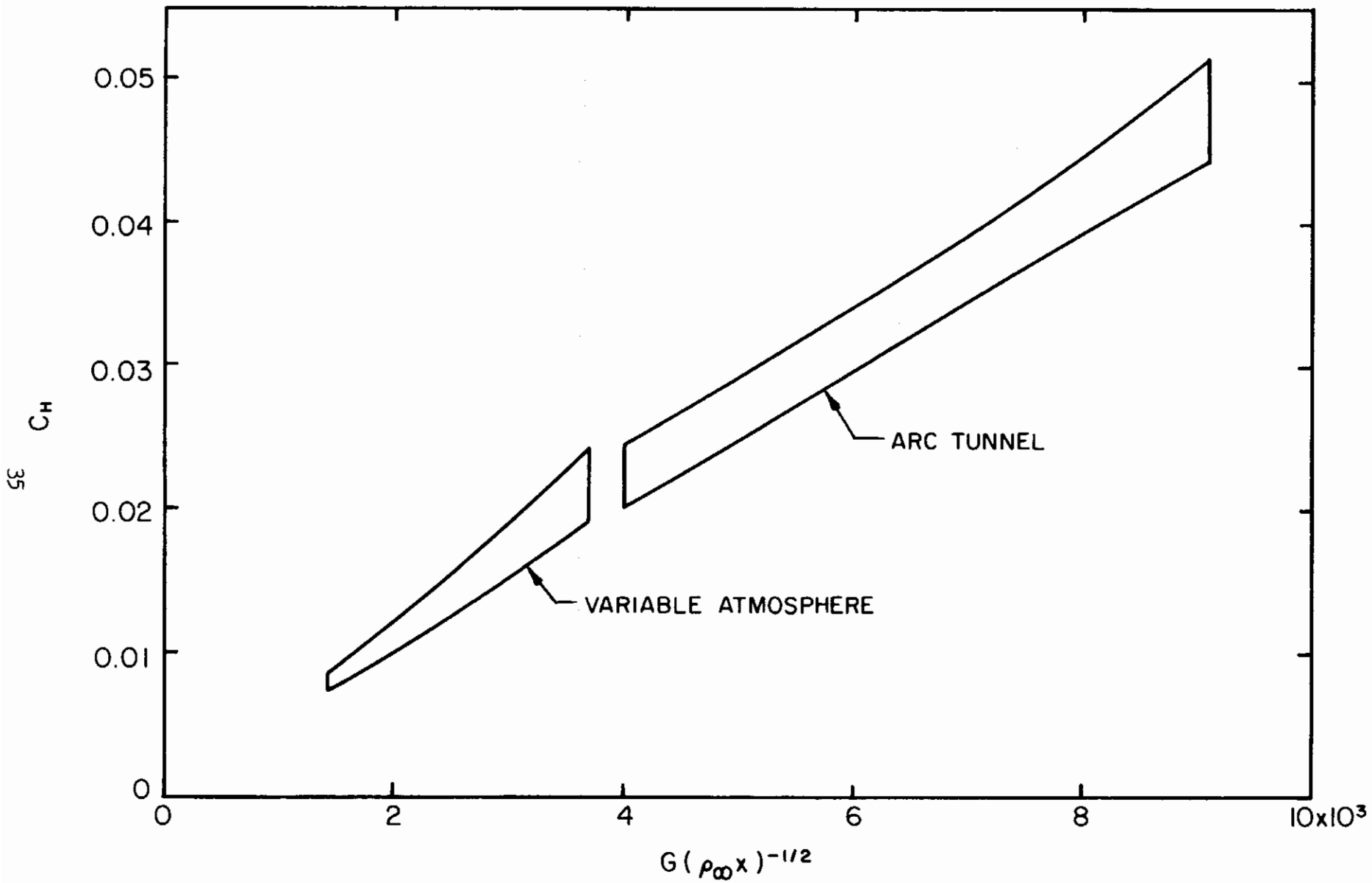

Fig. 11 - Heat Transfer Rate Coefficient on a 10°-Half Angle Cone in Variable Atmosphere and Arc Tunnels

been obtained simultaneously or under like test conditions on similar models can be compared on this basis. In some cases where surface pressure data are not available, realistic estimates can be made. This has been done to reduce the variable atmosphere 10°-cone heat transfer data by calculating the boundary layer displacement growth on a flat plate at $\alpha = 10°$ from the measured pressure, reducing this displacement angle by the Mangler factor, $\sqrt{3}$, and recalculating the cone pressure with Eq. (3). In all of the other results of Fig. 12, the measured pressure was used to reduce the data to the form of Eq. (43). Included in Fig. 12 are the sharp plate, variable-atmosphere data of the present tests, where the line shown is a data average covering variations in composition and angles of attack of 0°, 5° and 10°. A single average curve for the shock tunnel results of Ref. 29 is included where no systematic variation was observed for $\alpha = 0$, 5, and 10°. Additional shock tunnel data from Ref. 30 is shown for 9° cones. The hotshot tunnel data on a sharp plate at zero angle-of-attack from Ref. 31 was obtained in nitrogen at Mach 20. Finally, we include the 10°-cone data in an arc tunnel from the present series of tests. The arc tunnel flat plate results are not included because surface pressures under similar conditions were not available.

All of the curves in Fig. 12 are data averages from experiments which, in general, exhibit a scatter of ± 10% about the average. Within this variability, the results suggest that the hypersonic heat transfer at a point on planar and axisymmetric bodies as reduced by the surface pressure according to Eq. 43 is primarily a function of freestream density. This is not to imply that the more familiar dependence on Reynolds number is not valid. However, it is the local reference-property Reynolds number that is the controlling parameter and not a Reynolds number based on freestream properties. By not imposing the constraint that the similarity parameter in terms of free properties be nondimensional, for example, some combination of freestream Mach number and Reynolds number, we obtain a much simplified dependence on the dimensional combination $\rho_\infty x$.

V. CONCLUDING REMARKS

This study has shown that the hypersonic equations for the inviscid and viscous flow fields about slender bodies can be formulated with a minimal dependence on Mach number. Within the limitations of hypersonic small-disturbance theory the only need to consider Mach number at all is in the estimate of a wind tunnel freestream pressure. Errors involved in this estimate are of second order in importance and in the hypersonic limit, become negligible. This result, which is of use in situations where Mach number becomes an ill-defined parameter, contrasts with the usual theoretical formulations for hypersonic flow where Mach number is made a dominant parameter.

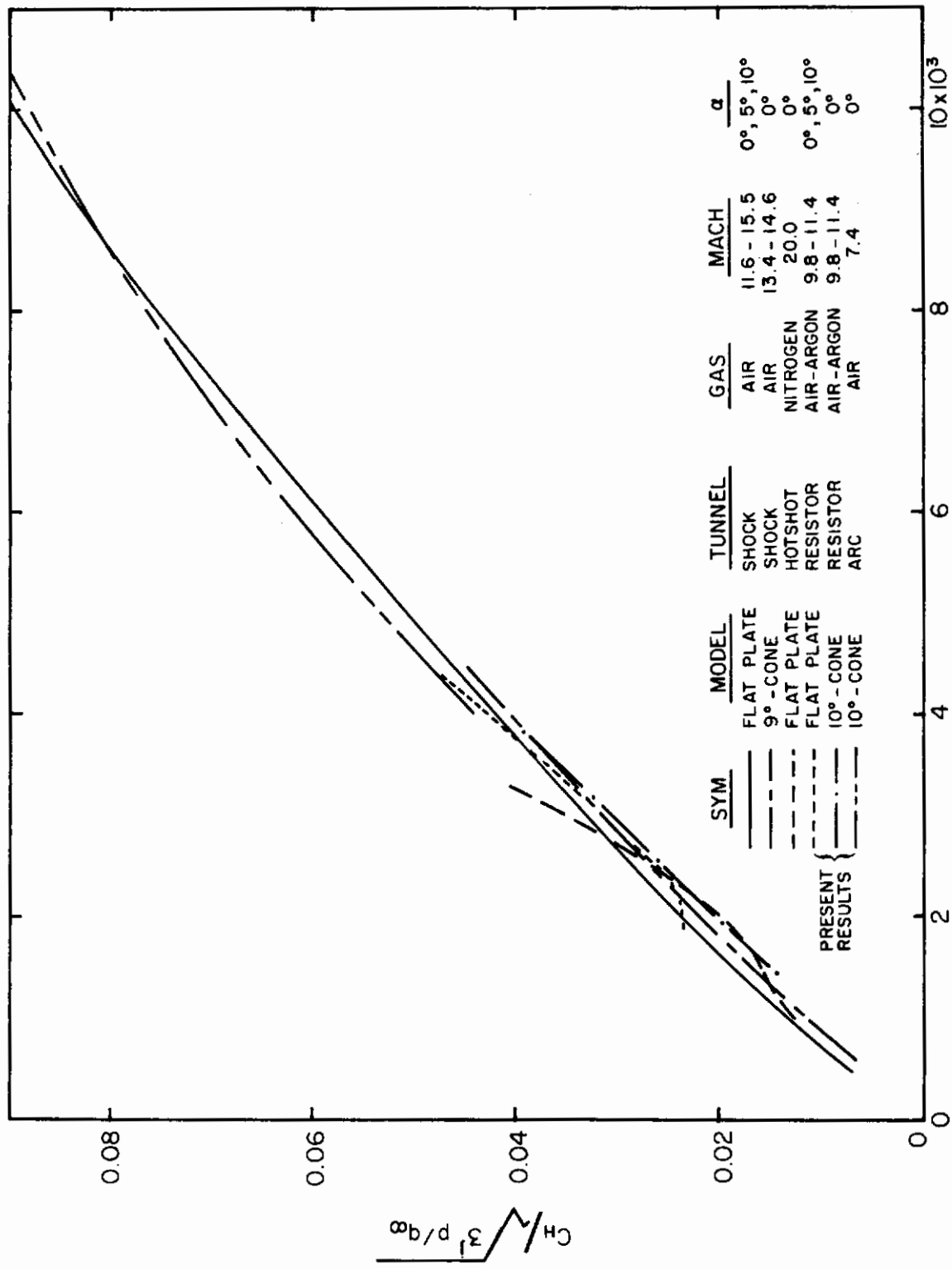

Fig. 12 - Global Comparison of Heat Transfer to Slender Bodies in Hypersonic Flow

For variable composition or nonequilibrium atmospheres, the inviscid and viscous equations can be developed in a form in which the thermodynamic and transport properties of the gas appear explicitly. For the inviscid small-disturbance flow field, this dependence reduces to variations in the freestream ratio of specific heats which appears explicitly in the equations for wedge and cone flows, (Eqs. (2) and (3)). In many cases, these equations adequately describe the aerodynamics of more generalized planar and axisymmetric shapes through the application of tangent-wedge and tangent-cone theories. For the viscous equations we can bring out the explicit dependence on the thermodynamic and transport properties of the atmosphere by use of the reference property transformation of the Blasius result expressed in terms of the growth rate of the boundary layer displacement thickness. The Sutherland relation for the temperature dependence of viscosity is used, i.e., the basic square root dependence for hard elastic spheres plus a correction term to account for attractive forces in a molecular encounter. As a simplification, the correction factor for attractive forces is small at the reference temperatures of interest and is taken throughout as that for air. With these assumptions, the gas properties can be factored out of the viscous equations to form parameters which account for variations in the composition of the atmosphere and which, for convenience, reduce to unity in the free flight case. Although the pressure gradient term is neglected in the boundary layer growth equation, the upstream pressure history is accounted for by a stretched axial coordinate which produces local flat plate similarity. A further simplification is possible when the pressure variation can be approximated in power law form. In this case, the boundary layer growth may be described in terms of the physical streamwise coordinate.

The inviscid flow field is coupled to the boundary layer by assuming that the flow is deflected through an angle which is the sum of the local inclination of the wall and the local angle of the boundary layer displacement thickness, i.e., $\theta = \theta_w + d\delta^*/dx$. For a given configuration, the inviscid pressure equation and the boundary layer growth equation give two equations in the two unknowns p/q_∞ and $d\delta^*/dx$. An explicit solution of these equations proves fruitful only for a sharp flat plate at zero angle-of-attack. In addition to the viscous equation for the boundary layer growth rate which couples with the inviscid flow equation, the skin friction coefficient, and the heat transfer rate coefficient developed from Reynolds analogy are given by very simple expressions.

It was not the intent that the equations as formulated for this study provide theoretical predictions of viscous induced pressure and hypersonic heat transfer but rather that they bring out the significant similarity parameters, including explicitly the effects of variable composition and nonequilibirum atmsopheres. Nevertheless, in addition to providing realistic corrections for variable atmospheres, the results provide reasonable estimates for pressure and heat transfer.

The experimental data covering a wide range of Mach number and gas composition indicate that the viscous induced pressure on a slender body in hypersonic flow is mainly a function of the freestream density and wall temperature (or T_w/T_o) with predictable secondary effects of variable gas composition and upstream pressure history. It appears that all of these factors should be included in the analysis of surface pressure; however, the heat transfer rate coefficient after being reduced by the actual surface pressure in accordance with Eq. (43) is determined almost entirely by the freestream density with a small correction for the effects of variable atmospheres.

REFERENCES

1. Petrie, S. L. and Gregorek, G. M., "Simulation of Blunt-Body Pressure Distributions," AFFDL-TR-66-49, 1966.

2. Petrie, S. L., and Gregorek, G. M., "A Summary of Similitude Studies for High Enthalpy Hypersonic Test Facilities," AFFDL-TR-66-74, 1966.

3. Tsien, H. S., "Similarity Law of Hypersonic Flow," J. Math. Phys., Vol. 25, pp. 247-251, 1946.

4. Hayes, W. D., "On Hypersonic Similitude," Quart. Appl. Math., Vol. 5, pp. 105-196, 1947.

5. Goldworthy, F. A., "Two-Dimensional Rotational Flow at High Mach Number Past Thin Airfoils," Quart. J. Mech. Appl. Math., Vol. 5, pp. 54-63, 1952.

6. Van Dyke, M. D., "Application of Hypersonic Small-Disturbance Theory," J. Aeronautical Sci., Vol. 21, No. 3, pp. 179-186, March 1954; NACA TR 1194; NACA TN 3173.

7. Cheng, H. K., "Similitude of Hypersonic Real-Gas Flows Over Slender Bodies with Blunted Noses," J. Aerospace Sci. 26, 575-585, 1959.

8. Inger, G. R., "Similitude of Hypersonic Flows Over Slender Bodies in Nonequilibrium Dissociated Gases," AIAA Journal, Vol. 1, No. 1, January 1963.

9. Lees, L., and Probstein, R. F., "Hypersonic Flows of a Viscous Fluid," Monograph, 1953, (AD No. 218755).

10. Hayes, W. D., and Probstein, R. F., "Viscous Hypersonic Similitude," J. Aero. Sci., Vol. 26, No. 12, pp. 815-824, December 1959.

11. Cheng, H. K., Hall, J. G., Golian, T. C., and Hertzbeg, A., "Boundary-Layer Displacement and Leading-Edge Effects in High Temperature Hypersonic Flow," J. Aerospace Sci., 18, pp. 353-381, May 1961.

12. Moore, F. K., "On Local Flat-Plate Similarity in the Hypersonic Boundary Layer," J. Aero. Sci., Vol. 28, No. 10, pp. 753-762, October 1961.

13. Harney, D. J., "Slender Body Aerodynamic Testing Potential of High Energy Wind Tunnels," AIAA Paper No. 68-383, AIAA 3rd Aerodynamic Testing Confernece, April 8-10, 1968.

14. Linnell, R. D., "Two-Dimensional Airfoils in Hypersonic Flows," J. Aero Sci., Vol. 16, No. 1, pp. 22-30, January 1949.

15. Patterson, G. N., Molecular Flow of Gases, John Wiley and Sons, New York, 1956.

16. Petrie, S. L., Fishburne, E. S., and Pierce, G. A., "Thermochemical Analysis of An Expanded Air Plasma," The Ohio State University, AFFDL-TR-64-191, 1964.

17. Eckert, E. R. G., Ibele, W. E. and Irvine, T. F., Jr., "Prandtl Number, Thermal Conductivity and Viscosity of Air-Helium Mixtures," NASA TN D-533, Sept. 1960.

18. Dorrance, W. H., Viscous Hypersonic Flow, McGraw-Hill, New York, 1962.

19. Hirschfelder, J. O., Curtis, C. F., and Bird, R. B., Molecular Theory of Gases and Liquids, John Wiley and Sons, New York, 1954.

20. Bray, K. N. C., "Simplified Sudden-Freezing Analysis for Non-equilibrium Nozzle Flows," ARS J. Vol. 31, No. 6, 831-834, June 1961.

21. Lordi, J. A., and Mates, R. E., "Nonequilibrium Effects of High-Enthalpy Expansions of Air," AIAA J., Vol. 3, No. 10, 1972-1974, October 1965.

22. Harris, C. J., and Warren, W. R., "Correlation of Nonequilibrium Chemical Properties of Expanding Air Flows," G. E. Space Sciences Laboratory, R64SD92, December 1964.

23. Harney, D. J., "Similarity of Nonequilibrium Expansions in Hypersonic Nozzles," AF Flight Dynamic Lab, FDM-TM-67-1, May 1967.

24. Ring, L. E., and Johnson, P. W., "Correlation and Prediction of Air Nonequilibrium in Nozzles," AIAA Paper No. 68-378, AIAA 3rd Aerodynamic Testing Conference, April 8-10, 1968.

25. Gregorek, G. M., and Lee, J. D., "Heat Transfer Measurements in Hypersonic Low Density Flows With Phase Change Coatings," ARL 68-0004, January 1968.

26. Kinslow, M., and Arney, G. D., Jr., "Thermo-Molecular Pressure Effects in Tubes and at Orifices," AGARDograph 119, August 1967.

27. Kendall, J. M., Jr., "Experimental Investigation of Leading-Edge Shock Wave-Boundary Layer Interaction at Mach 5.8," J. Aeronaut. Sci. 24, pp. 47-56, January 1957.

28. Feldhuhn, R. H., "An Experimental Investigation of the Effects of Leading Edge Reynolds Number and Angle of Attack on the Flow of Helium over a Flat Plate at M = 16.35," M. S. Thesis, Princeton University, July 1965.

29. Wallace, J. E., and Burke, A. F., "Skin Friction, Heat Transfer and Pressure Distributions over a Flat Plate and Highly Swept Delta Wings with Sharp and Blunt Leading Edges at Angles of Attack in Hypersonic Flow," ASD-TDR-63-772, 1963.

30. Wilkinson, D. B., and Harrington, S. A., "Hypersonic Force, Pressure, and Heat Transfer Investigation of Sharp and Blunt Slender Cones," AEDC-TDR-63-177, August 1963.

31. Harvey, W. D., "Effects of Leading-Edge Bluntness on Pressure and Heat-Transfer Measurements Over a Flat Plate at a Mach Number of 20," NASA TN D-2846, October 1965.

Unclassified
Security Classification

DOCUMENT CONTROL DATA - R & D

(Security classification of title, body of abstract and indexing annotation must be entered when the overall report is classified)

1. ORIGINATING ACTIVITY (Corporate author)	2a. REPORT SECURITY CLASSIFICATION
The Ohio State University Research Foundation 1314 Kinnear Rd. Columbus, Ohio 43212	Unclassified
	2b. GROUP N/A

3. REPORT TITLE

HYPERSONIC SURFACE PRESSURE AND HEAT TRANSFER ON SLENDER BODIES IN VARIABLE COMPOSITION AND NONEQUILIBRIUM ATMOSPHERES

4. DESCRIPTIVE NOTES (Type of report and inclusive dates)

Final Report - September 1, 1968 through September 30, 1969

5. AUTHOR(S) (First name, middle initial, last name)

D. J. Harney; S. L. Petrie

6. REPORT DATE	7a. TOTAL NO. OF PAGES	7b. NO. OF REFS
April 1970	50	31

8a. CONTRACT OR GRANT NO.	9a. ORIGINATOR'S REPORT NUMBER(S)
AF33(615)-69-C-1077 b. PROJECT NO. 1426 c. Task No. 142604 d.	9b. OTHER REPORT NO(S) (Any other numbers that may be assigned this report) AFFDL-TR-70-31

10. DISTRIBUTION STATEMENT

This document has been approved for public release and sale; its distribution is unlimited.

11. SUPPLEMENTARY NOTES	12. SPONSORING MILITARY ACTIVITY
	Department of the Air Force Air Force Flight Dynamics Laboratory(AFSC) Wright-Patterson Air Force Base, Ohio 45433

13. ABSTRACT

The aerodynamic testing of slender bodies in high energy wind tunnels is complicated by the effects of the nonequilibrium expansion process in the wind tunnel nozzle. The atmosphere that a model sees varies in composition dependent upon the degree of nonequilibrium. This variation affects the inviscid flow field through changes in the ratio of specific heats and the viscous equations by changes in the transport as well as the thermodynamic properties of the gas. Within the limitations of hypersonic small disturbance theory the inviscid and viscous equations are formulated with a minimal dependence on Mach number and in a way that brings out their explicit dependence on the thermodynamic and transport properties of the gas. The resulting gas property parameters then are calculated for air-argon mixtures, air-helium mixtures, and frozen dissociate air. These parameters appear to provide a realistic estimate of the effect of a variable atmosphere on surface pressure and heat transfer based on the current series of tests on sharp cones and flat plates in air-argon mixtures and in a low pressure arc tunnel. In addition, the present experiments and comparative experiments in other facilities demonstrate a result of more general interest; namely, that the Mach number is not a dominant parameter in slender body viscous hypersonic aerodynamics.

DD FORM 1 NOV 65 1473

Unclassified
Security Classification

14. KEY WORDS	LINK A		LINK B		LINK C	
	ROLE	WT	ROLE	WT	ROLE	WT
Slender bodies						
High energy wind tunnels						
Nonequilibrium						
Inviscid flow						
Small disturbance theory						
Air-Argon mixtures						
Air-Helium mixtures						
Frozen dissociate air						
Hypersonic aerodynamics						